의학박사 학위논문

# The role of SIRT1 in avoiding AIM2-mediated antiviral defense in cervical cancer

# 자궁경부암에서 AIM2 를 매개체로 하는 항바이러스 방어 기전 회피에 대한 SIRT1 의 역할

2018 년 8 월

서울대학교 대학원

의과학과 약리학전공

소 대 호

A thesis of the Degree of Doctor of Philosophy

# 자궁경부암에서 AIM2 를 매개체로 하는 항바이러스 방어 기전 회피에 대한 SIRT1 의 역할

# The role of SIRT1 in avoiding AIM2-mediated antiviral defense in cervical cancer

August 2018

The Department of Biomedical Science,
Seoul National University
College of Medicine

Dae-Ho So

# ABSTRACT

Mammalian cells are equipped with antiviral defense system. To survive and grow, human papillomavirus (HPV)-infected cervical cancer cells must overcome this host defense system. However, the precise mechanism whereby cervical cancer cells effective evade the defense system is not fully understood. I noted that Sirtuin 1 (SIRT1) is overexpressed in HPV-infected cervical cancer cells and hypothesized that SIRT1 plays a significant role in survival of cervical cancer. Here, I found that cervical cancer cells undergo massive death by SIRT1 knockdown, but this effect is reversed by SIRT1 restoration. SIRT1-knocked-down cells showed representative features of pyroptosis, as well as highly expressed absent in melanoma 2 (AIM2) and its downstream genes related to the inflammasome response. Mechanistically, SIRT1 repressed the NF-κB-driven transcription of the *AIM2* gene by destabilizing the RELB mRNA. Interestingly, pyroptotic death signaling in SIRT1-knocked-down cells was transmitted to naïve cervical cancer cells, which was mediated by extracellular vesicles carrying AIM2 inflammasome proteins. Furthermore, the growth of

cervical cancer xenorgafts was noticeably inhibited by either SIRT1-targeting siRNAs or SIRT1 knockdown-derived extracellular vesicles. Immunohistochemical analyses showed that SIRT1 expression correlates with poor clinical outcome in cervical cancer. In conclusion, SIRT1 enables HPV-infected cervical cancer cells to continue growing by nullifying AIM2 inflammasome-mediated immunity. Without SIRT1, cervical cancer cells can no longer survive because of the derepression of the AIM2 inflammasome. SIRT1 could be a remarkable target for cervical cancer therapy.

---

Keywords: Cervical cancer, Human papillomavirus, Sirtuin 1, Absent In Melanoma 2, Inflammasome, Pyroptosis

Student number: 2012-23667

# CONTENTS

Abstract ..... 1

Contents ..... 3

List of tables and figures ..... 4

List of abbreviations ..... 7

Introduction ..... 8

Materials and Methods ..... 13

Results ..... 28

Figures ..... 41

Discussion ..... 109

References ..... 114

Abstract in Korean ..... 120

# LIST OF TABLES AND FIGURES

Figure 1. SIRT1 is vital for cell survival in cervical cancer..... 41
Figure 2. Effects of SIRT1 knockdown on cervical cancer cell growth..... 43
Figure 3. Effects of SIRT1 knockdown on several cancer cells growth..... 45
Figure 4. Cell cycle analyses in diverse cancer cells..... 47
Figure 5. Cell cycle pathway study in SIRT1 knockdown cells..... 49
Figure 6. Cell death analyses in cervical cancer cell ..... 50
Figure 7. SIRT1 knockdown induces non-apoptotic cell death in cervical cancer cell..... 51
Figure 8. SIRT1 knockdown induces cervical cancer cell damage in an autophagy independent-manner ..... 52
Figure 9. cDNA microarray analysis of the SIRT1 knockdown in cervical cancer cell..... 53
Figure 10. Heatmap analyses of the significant gene sets in SIRT1 knockdown ..... 55
Figure 11. Negative correlation between SIRT1 and AIM2 in cervical cancer..... 57
Figure 12. The acidification of media occurred faster in SIRT1 knockdown cell ..... 59
Figure 13. Effects of SIRT1 knockdown on glucose energy metabolism in cervical cancer cell ..... 60
Figure 14. SIRT1 knockdown provokes morphological changes in cervical cancer cell..... 62

Figure 15. SIRT1 knockdown causes an imbalance of the ionic homeostasis ..... 64
Figure 16. SIRT1 knockdown leads to cell death by activating the AIM2 inflammasome ..... 66
Figure 17. Caspase-1 inhibitor rescues cell growth in SIRT1 knockdown cancer cell ..... 68
Figure 18. Downstream genes of the AIM2 inflammasome ..... 70
Figure 19. SIRT1 represses the transcription of the *AIM2* gene .... 71
Figure 20. SIRT1 protects cervical cancer by suppressing the NF-κB- mediated AIM2 expression ..... 73
Figure 21. SIRT1 destabilizes the RELB mRNA ..... 75
Figure 22. SIRT1 promotes cervical cancer cell survival in a deacetylase−independent manner ..... 77
Figure 23. Effects of SIRT1 deacetylase inhibitors on cancer cell growth ..... 79
Figure 24. SIRT1 knockdown-derived conditioned media inhibit cervical cancer cell growth ..... 81
Figure 25. Intercellular transmission of pyroptosis under SIRT1 knockdown ..... 83
Figure 26. SIRT1 knockdown-derived conditioned media trigger pyroptotic events ..... 84
Figure 27. SIRT1 knockdown-derived conditioned media causes an imbalance of the ionic homeostasis ..... 86
Figure 28. Identifying the pyroptosis-transmitting factor in SIRT1 knockdown-derived condition media ..... 88
Figure 29. Inflammasomal components are transmitted through extracellular vesicles ..... 90

Figure 30. Inflammasome-mediated pyroptosis is propagated via extracellular vesicles..... 92
Figure 31. Anticancer effects of SIRT1-targeting siRNA and SIRT1 knockdown-derived extracellular vesicles..... 94
Figure 32. Parameters in xenografted SiHa tumors..... 96
Figure 33. Activation of AIM2 inflammasome in xenografted tumors..... 98
Figure 34. Immunohistochemical analyses of AIM2 inflammasome-related proteins in siRNA injected tumors..... 100
Figure 35. Immunohistochemical analyses of AIM2 inflammasome-related proteins in SIRT1 knockdown-derived extracellular vesicles injected tumors..... 102
Figure 36. Transmission electron microscopy images of tumors injected with siRNAs..... 104
Figure 37. High expression of SIRT1 is associated with poor survival in cervical cancer patients..... 105
Figure 38. Negative correlation between SIRT1 and AIM2 in patient tissue of cervical cancer..... 107
Figure 39. Graphical summary of SIRT1 knockdown effect on cervical cancer..... 108

# LIST OF ABBREVIATIONS

AIM2: Absent in melanoma 2

Cas−1: Caspase−1

ChIP: Chromatin immunoprecipitation

EV: Extracellular vesicle

GFP: Green fluorescent protein

GSEA: Gene Set Enrichment Analysis

HPV: Human papillomavirus

HSP: Heat shock protein

NAD: Nicotinamide adenine dinucleotide

ORF: Open reading frame

Sir2: Silent information regulatory 2

SIRT1: Sirtuin 1

STAT1: Signal transducer and activator of transcription 1

TCGA: The Cancer Genomic Atlas

TEM: Transmission Electron Microscopy

# INTRODUCTION

Cervical cancer is the fourth most common cancer in women worldwide.[1] Half of all women diagnosed with the disease are between 35 and 55 years of age. About 85% of the deaths from cervical cancer occur in underdeveloped or developing counties. Almost all cases of cervical cancer are caused by infection with the human papillomavirus (HPV). Generally, HPV infections are transient, harmless, and will be cleared spontaneously. However, in some case continuous infection will result in the development of the malignant conditions of cervical epithelial neoplasia.

HPV is a non-enveloped DNA virus containing a circular, double-stranded viral genome. More than 100 types of human papillomavirus have been identified, including 13 high-risk types of HPVs, HPV-16 and HPV-18 account for approximately 70% of all cervical cancers.[2] The integration of the HPV genome into the host genome is generally observed in cervical cancers, and this is accompanied by long-lasting expression of viral oncogenes.[3] Viral genome integration causes genomic instability in host cells, provoking the activation of

cellular defense mechanisms. Host cells are equipped with antiviral immune systems, such as the interferon signaling pathways, T-cell activation, and the production of proinflammatory cytokines.[4] Despite these challenges, HPV-infected host cells survive by evading antiviral defense system and eventually become transformed to cancer cells. The viral oncogenes E6 and E7 have been known to contribute to the malignant transformation of epithelial cells by inactivating and degrading tumor suppressors TP53 and RBs.[5,6] TP53 has an important role in protecting genomic integrity by forcing apoptosis or inducing cell cycle arrest until errors in DNA replication can be repaired. E6 targets TP53 for degradation via the ubiquitin pathway, preventing apoptosis and enabling potentially transformed cells to replicate. E7 contributes to oncogenesis through its interaction with the retinoblastoma family. E7 binds these proteins and target them for degradation. However, the precise mechanism underlying the survival and malignant transformation of HPV-infected cells is not fully understood.

Sir2 (silent information regulatory 2) was initially found in yeasts as a longevity-related protein.[7] Seven mammalian

homologs of yeast Sir2, named Sirtuins (SIRT1-7), have been identified to date. Among them, SIRT1 is the most similar to yeast Sir2 in structure and its functionality has been intensively investigated. SIRT1 is the $NAD^+$-dependent protein deacetylase that removes the acetyl moiety from acetylated lysine residues in histone and nonhistone proteins.[8] Because it targets a variety of cellular proteins, SIRT1 participates in diverse biological processes, such as the cell cycle, energy and nutrient metabolism, inflammatory processes, and DNA damage responses.[9-12] SIRT1 was also demonstrated to suppress immune responses by deacetylating and inactivating the p65/RelA subunit of NF-κB.[13] However, the role of SIRT1 in cancer development remains controversial because conflicting data on the effects of SIRT1 on tumorigenesis and tumor progression have been reported thus far. Recently, several studies have demonstrated that SIRT1 is highly expressed in HPV-infected cervical cancers, and it was required for the survival and growth of cervical cancer cells.[14-16] However, the molecular function of SIRT1 in cervical cancer cells has not been explored. Given that HPV-infected cells must escape from antiviral immunity to survive, I hypothesized that SIRT1

overexpression in cervical cancer cells counteracts the antiviral system. In this study, I found that SIRT1 protects HPV-infected cervical cancer cells from the absent in melanoma 2 (AIM2) inflammasome—an intracellular immunity system against DNA viruses.

Absent in melanoma (AIM2) is a member of the interferon-inducible PYHIN family. It is located in the cytosol and senses dsDNA of viral or bacterial origin. Upon binding to DNA, AIM2 assembles a multi-protein complex called the inflammasome, which drives pyroptosis. Pyroptosis is morphologically and mechanistically distinct from other forms of cell death. Caspase-1 dependence is a defining feature of pyroptosis, and caspase-1 in the enzyme that mediates this process of cell death. Pyroptosis features rapid plasma-membrane rupture and release of proinflammatory intracellular contents. Cell lysis during pyroptosis results from caspase-1-mediated processes. Caspase-1-dependent plasma membrane pores dissipate cellular ionic gradients, producing a net increased osmotic pressure, water influx, cell welling and, eventually, osmotic lysis and release of inflammatory intracellular contents. When SIRT1 was knocked down, cervical cancer cells underwent

massive death due to the intercellular transmission of inflammasome-induced pyroptosis. I also demonstrated *in vivo* that SIRT1 could be a potential target for cervical cancer therapy.

# MATERIALS AND METHODS

## Cell Culture

Human cervical cancer cell lines SiHa, ME-180, CaSki, SNU-17, and HeLa were purchased from the Korean Cell Line Bank (Seoul, Korea). SiHa and HeLa were cultured in Dulbecco's modified Eagle medium (Sigma, St. Louis, MO), and ME-180, CaSki, SNU-17 were in RPMI-1640 medium (Sigma). All media contain 10% heat-inactivated fetal bovine serum and antibiotics. Cells were grown at 37℃ under 5% $CO_2$.

## Small Interfering RNAs, Plasmids and Transfection

Small interfering RNAs (siRNAs) were provided by Integrated DNA Technologies (Coralville, IA). The sequences (5' to 3') of siRNAs are AGUACAAACUUCUAGGAAUGUUGAA for si-SIRT1; CCAGAAAGGUGUAAUAUUUAUAGGT for si-SIRT1/3' UTR; GAGAUAAGGUUCGACUUACAUUCTT for si-AIM2. The SIRT1-targeting siRNA Pool was purchased from siTOOLs Biotech (Planegg, Germany). The plasmids expressing SIRT1 and its mutants were kindly given by Dr. Ja-Eun Kim (Kyung Hee University, Korea). Other plasmids were

constructed by RT-PCR and blunt-end ligation. For transient gene silencing or protein expression, approximately 40% confluent cells were transfected with siRNAs (40 nM) or plasmids (1 μg/mL) using Lipofectamine RNAiMax or Lipofectamine 3000 (Thermo Fisher Scientific, Waltham, MA).

### Immunoblotting

Proteins were electrophoresed on sodium dodecyl sulfate-polyacrylamide gels and transferred to Immobilon-P (Merck Millipore, Billerica, MA). Membranes were incubated with primary antibodies overnight at 4℃, incubated with horseradish-peroxidase-conjugated secondary antibodies (1:5000) for 1 hour at room temperature, and visualized using Luminata ECL Western Blotting Detection reagent (Merck Millipore).

### Reverse-Transcription and Quantitative Polymerase Chain Reaction

Total RNAs were isolated using TRIzol reagent (Thermo Fisher Scientific) and reverse-transcribed to complementary cDNAs using the Tetro cDNA Synthesis Kit (Bioline, London,

UK). Real-time PCR analyses were performed in triplicate with TOPreal qPCR 2X PreMIX (Enzynomics, Daejeon, Korea) using CFX Connect Real-Time PCR Detection System (Bio-Rad Laboratories, Hercules, CA). Serially diluted standard curves were included to quantify the samples. Data were analyzed using the CFX manager software (Bio-Rad Laboratories) and values were normalized to β-actin. The primer sequences (5' to 3') are GATGATTCAAAATGCTGGGG and TGACTTAGTGGCTTTGGTTT for AIM2 mRNA; GGACCTGACTGACTACCTCA and AGCTTCTCCTTAATGTCACG for β-actin mRNA; GAATTAACAAGGAAAGCGGG and TTGAACACAATGGCAATCTG for RelB mRNA; AGACGTTTCTCCTTCTCTGC and CTGTCAGGAGAAAGCTGAGG for RelB pre-mRNA.

## Reporter Assays

To analyze the activity of the *AIM2* gene promoter, Cells were co-transfected with the AIM2 promoter (-728 to -1 base pairs from the primary transcription site)-luciferase plasmid and the β-galactosidase plasmid. Luciferase activity was

analyzed using Lumat LB960 luminometer (Berthold Technologies, Bad Wildbad, Germany) and the value was divided by the galactosidase activity in the same sample to normalize transfection efficiency.

### Conditioned Media Preparation

SiHa cells ($4\times10^6$ cells in 100-mm dish) were transfected with 40 nM siRNA. After cells were incubated for 24 hours, the conditioned media were harvested and centrifuged at 1500xg for 10 minutes. The media were transferred to the Ultra 15 Centrifugal filter 100K (Millipore) and centrifuged at 5000xg for 30 minutes. The concentrated medium in the upper chamber was condensed with one over sixtieth. The volume of the concentrated medium was adjusted to the original volume with fresh DMEM.

### Extracellular Vesicles Isolation

The conditioned media were collected from SiHa cell and centrifuged at 3000xg for 15 minutes, mixed with ExoQuick precipitation reagent (System Biosciences, Mountain View, CA), and incubated at 4℃ for 12 hours. The mixture was centrifuged

at 1500xg for 30 minutes and supernatant was removed by aspiration, and the vesicle pellet was resuspended with 100 μL of phosphate buffered saline. Protein content in the extracellular vesicles was measured using a Pierce BCA protein assay kit (Thermo). The average extracellular vesicles yield was 200 μg from 10 mL conditioned media ($5\times10^6$ cells).

### Chromatin immunoprecipitation (ChIP)

Cells were fixed with 1% formaldehyde, lysed with 1% SDS, sonicated, and centrifuged. The RelB-containing chromatin complexes were precipitated using anti-RelB antibody and protein-G beads sequentially. Chromatin DNAs were extracted in the phenol/chloroform/isoamylalcohol mixture, and quantified by real-time PCR. For analysis, 1% of starting chromatin is used as input. Firstly, for adjusted input to 100%, 6.644 cycle was subtracted from the Ct value then, $100*2^{(\text{Adjusted input} - \text{Ct (IP)}}$ was used for calculated percent input.

### SIRT1 activity Assay

SIRT1 deacetylase activity was measured by using a SIRT1 Fluorometric Assay kit (Abcam, Cambridge, UK). SiHa cells

were treated with SIRT1 inhibitors (Sirtinol, Nicotinamide and EX-527) for 48 hours, and immunoprecipitated with anti-SIRT1 antibody (Santa Cruz Biotechnology) and Protein A agarose beads. The reaction was initiated with mixing fluoro-substrate peptide solution and beads. NAD dependent deacetylase activity was measured at Ex350 nm/Em460 nm using Infinite 200 Pro Elisa (Tecan, Mannedorf, Swiss).

### Transmission Electron Microscopy

Prepared samples were fixed overnight in a mixture of cold 2.5% glutaraldehyde in 0.1 M phosphate buffer (pH 7.2), and 2% paraformaldehyde in 0.1 M phosphate or cacodylate buffer (pH 7.2). Samples were post-fixed for 1.5 hours in 2% osmium tetroxide in 0.1 M phosphate or cacodylate buffer for 1.5 hours at room temperature. The samples were then washed briefly with deuterated $H_2O_2$, dehydrated throughout a graded 50, 60, 70, 80, 90, 95, and 100% ethanol (X2) series, infiltrated by using propylene oxide and EPON epoxy resin mixed and finally embedded with only epoxy resin. The epoxy resin-mixed samples were loaded into capsules and polymerized at 38℃ for 12 hours and 60℃ for 48 hours. Sections for light microscopy

were cut at 500 nm and stained with 1% toluidine blue for 45 seconds on a hot plate at 80℃. Thin sections were made using an ultramicrotome (RMC MT-XL) and collected on copper grid. Appropriate areas for thin sectioning were cut at 65 nm and stained with saturated 6% uranyl acetate and 4% lead citrate before examination with a transmission electron microscope (JEM-1400; Japan) at 80 Kv.

### Measurement of Intracellular $Ca^{2+}$

The intracellular $Ca^{2+}$ levels were measured using the fluorescence tracer Fura-2 AM. Cells were grown in a cover glass and loaded with 1 μM Fura-2 AM at 37 ° C for 30 minutes. Calcium-bound Fura-2 AM was excited at 340 and 380 nm and the emitted light was detected at 510 nm using Lambda DG-4 (Sutter Instruments) illuminator. Each fluorescence image was acquired on CoolSNAP HQ2 CCD camera (Photometrics, Tucson, AZ) controlled by MetaMorph 7.6 software.

### Measurement of Intracellular Lactate Level

Intracellular lactate level was measured by using a Lactate

Colorimetric Assay kit (BioVision, Milpitas, CA). Lactate is oxidized by lactate dehydrogenase to generate a product that interacts with a dye. Transfected SiHa cells were harvested and homogenized with assay buffer, then mixed with lactate enzyme and substrate. Lactate was measured at 450 nm in microplate reader (SoftMax Pro, Sunnyvale, CA). Lactate level was normalized to cell number and represented as a relative level from control cells.

### Measurement of Intracellular Pyruvate Level

Intracellular pyruvate level was measured by using a Pyruvate Colorimetric Assay kit (BioVision). Pyruvate is oxidized by pyruvate oxidase via enzyme reactions to generate color. Transfected SiHa cells were harvested and homogenized with assay buffer, then mixed with pyruvate probe and enzyme. Pyruvate was measured at 570 nm in microplate reader (SoftMax Pro). Pyruvate level was normalized to cell number and represented as a relative level from control cells.

### Measurement of Intracellular ATP Level

Intracellular ATP level was measured by using the

EnzyLight™ ADP/ATP Ratio assay kit (BioAssay Systems, Hayward, CA). In the presence of luciferase, ATP immediately reacts with substrate D-luciferin to produce light. Transfected or conditioned media treated SiHa cells were harvested and mixed with assay buffer containing substrate, cosubstrate and ATP enzyme. Then, ATP level was measured using Lumat LB960 luminometer and represented as a relative level from control cells.

### Caspase-3 Activity Assay

Caspase-3 activity was measured using the colorimetric caspase-3 assay kit (Sigma). In brief, the lysates from $1 \times 10^6$ cells were incubated in the reaction mixture containing the caspase-3 substrate acetyl-Asp-Glu-Val-Asp-p-nitroanilide (finally 200 μM) at 37℃ for 2 hours. The activity was assessed based on the absorbance at 405 nm using TECAN microplate reader.

### Cell Cycle Analysis

Cells were harvested and fixed in 75% ethanol for 30 minutes on ice. After washing with phosphate buffered saline, cells were

labeled with propidium iodide (0.05 mg/mL) and RNase (0.5 mg/mL) and incubated in the dark at 37℃ for 30 minutes. DNA contents were analyzed using flow cytometry (FACS Canto Ⅱ).

## Animal studies

All animal studies were performed according to an approved protocol (approve number, SNU-160622-2) from the Seoul National University Institutional Animal Care and Use Committee. Five weeks old, female nude mice (Balb/cSlc-nu/nu) were purchased from Japan SLC Inc. (Shizuoka, Japan) and housed in a specific pathogen-free room under temperature- and humidity-controlled conditions. SiHa cells ($5\times10^6$ cells/mouse) were subcutaneously inoculated in the flank of mouse. Tumor sizes were measured daily using a caliper, and calculated using the equation $a\times b^2/2$ (a, width at the widest point; b, perpendicular width). When tumor volume attains at 300 $mm^3$, mice were intratumoral injected with siRNA (10 μg per tumor) or extracellular vesicles (15 μg per tumor) once every 5 days or 3 days, respectively. The in vivo-jetPEI transfection reagent (Polyplus, New York, NY) was used for the intratumoral transfection of siRNAs.

### Immunohistochemistry in Human Cervical Cancer Tissues

Human cervical cancer tissue arrays were obtained from SuperBioChips Lab (Seoul, Korea). The tissue array contained 59 tumor specimens from cervical cancer patients, whose clinical data, including sex, age, TNM stage, and survival, were informed by the supplier. The tumor tissues were fixed with 4% paraformaldehyde, paraffin-embedded, and cut into 6 μm section slices. The arrays were rehydrated and autoclaved at 121℃ for 10 minutes in a citrate buffer (Dako) to retrieve antigen. They were incubated with 3% $H_2O_2$ for 10 minutes and with 10% bovine serum for 1 hour to block non-specific signals. Sections were incubated overnight at 4℃ with antibodies against SIRT1 (1:50; Santa Cruz Biotechnology), AIM2 (1:50; Santa Cruz Biotechnology), Caspase-1 (1:50; Cell Signaling Technology), Caspase-1 p20 (1:50; Santa Cruz Biotechnology). Immune complexes were visualized using the Vectastatin ABC kit (Vector Laboratories) and the DAB detection kit (Dako). Finally, all sections were counterstained with hematoxylin. To score protein levels, two examiners observed 4 high-power fields on each slide. Protein expression was semi-

quantitatively analyzed using histoscore, which reflects the intensity of staining (graded as: 0, non-staining; 1, weak; 2, moderate; 3, strong) and the percentage of positive cells. The range of possible scores was from 0 to 300.

### cDNA microarray

High-quality RNA samples were processed for genome-wide transcript expression using Agilent Human GE 4 × 44K V2 microarrays (Agilent Technologies Inc.). The Low Input Quick Amp Labeling Kit (Agilent Technologies Inc.) was used for labeling and hybridization. The control and test samples were labeled with the aid of T7 RNA polymerase in the presence of Cy3-CTP and Cy5-CTP, respectively. The Cy3-labeled and Cy5-labeled cRNAs were purified using RNeasy MiniElute Cleanup kit (Qiagen). The yield and label incorporation efficiencies were measured with the aid of a spectrophotometer (NanoDrop Lite, Thermo Fisher Scientific, Inc). Each 825 ng of Cy3-labeled and cy5-labeled cRNA was mixed and fragmented at 60° C for 30 min (Agilent Gene Expression Hybridization Kit) and then hybridized to human whole genome 4×44K oligo microarray v2 slide (Agilent Technologies Inc.) at 65° C for 17

h. After hybridization, the arrays were washed consecutively by using Gene Expression Wash Pack (Agilent Technologies). Fluorescence images of the hybridized arrays were generated using the Agilent DNA Microarray Scanner, and the intensities were extracted with Agilent Feature Extraction software ver.10.7.3.1.

The data quantification was performed using Agilent Feature Extraction software 10.7 (Agilent Technology, USA). The average fluorescence intensity for each spot was calculated and local background was subtracted. All data normalization and selection of fold-changed genes were performed using GeneSpringGX 7.3.1 (Agilent Technology, USA). Genes were filtered with removing flag-out genes in each experiment. Intensity-dependent normalization (LOWESS) was performed, where the ratio was reduced to the residual of the Lowess fit of the intensity vs. ratio curve. The averages of normalized ratios were calculated by dividing the average of normalized signal channel intensity by the average of normalized control channel intensity. Functional annotation of genes was performed according to Gene Ontology™ Consortium (http://www.geneontology.org/index.shtml) by GeneSpringGX

7.3.1.

### Gene Set Enrichment Analysis

The TCGA dataset for human cervical cancer tissues was downloaded from the cBioPortal for cancer genomics (www.cbioportal.org), where mRNA data were obtained in the form of normalized RSEM value and divided into two groups depending on SIRT1 mRNA expression levels. Gene set enrichment analysis (GSEA) was performed using inflammasome-related genes in the MSigDB databases C2 curated gene sets or gene sets classified by DAVID ontology analysis. The gene sets with $P<0.05$ and false discovery rate (FDR) < 0.1 were considered significantly enriched. GSEA was performed according to the modified $t$-statistics from the comparison analysis using GSEA algorithm v2.0 (http://www.broadinstitute.org/gsea).

### Statistical Analysis

Statistical analyses were performed using the SPSS statistics program version 19 (Chigago, IL). Data were analyzed using Mann-Whitney U test for nonparametric test or Student's t-

test for parametric test. Overall survival curves of cervical cancer patients in tissue arrays were plotted by Kaplan-Meier method, and the difference in overall survival between SIRT1 high and low groups was analyzed using Log-Rank test. All statistical tests were two-sided, and significance was considered when the P value was less than 0.05.

# RESULTS

## SIRT1 is essential for cell survival in cervical cancer.

Of the 13 cancer cell lines, SiHa (HPV-infected cervical cancer) was found to express SIRT1 most abundantly (Figure 1A and B). To investigate the role of SIRT1 in cervical cancer cells, I transfected five different cervical cancer cell lines with a SIRT1-silencing short-interfering RNA (si-SIRT1; Figure 1C and D) and further cultured them for 2 days. Surprisingly, squamous carcinoma cell-lines (SiHa, CaSki, SNU17, and ME-180) were poorly proliferative under SIRT1 knockdown conditions, but an adenocarcinoma cell-line HeLa was not (Figures 1E and 2A). To rule out the off-target effects of the siRNA, I transfected the siRNA Pool system (siPool) into SiHa cells. This system also inhibited SiHa cell growth, which was reversed by SIRT1 restoration (Figure 2B). By contrast, cell growth in other types of cancer was seldom affected by SIRT1 knockdown (Figure 3A-C). Next, to confirm cell growth inhibition in SIRT1 knockdown cervical cancer cells, I performed cell cycle analyses. The results showed that, cervical cancer cells occurred cell cycle arrest in SIRT1

knockdown, however, other types of cancer cells were rarely affected by SIRT1 knockdown (Figure 4). S-phase arrest was occurred in half of the cervical cancer cells in SIRT1 knockdown and caused by phosphorylation of Chk1(Ser 345) (Figure 5A). However, it was for nothing in other cell cycle related pathway, such as ERK or FOXM1, affected by SIRT1 (Figure 5B). I performed flow cytometry analyses, to determine the cell death mechanism, that induced by SIRT1 knockdown in cervical cancer. However, the proportions of apoptosis and necrosis were neither substantial nor consistent in five cervical cancer cell lines (Figure 6). Moreover, apoptotic markers were not clearly induced by SIRT1 knockdown (Figure 7). Given a previous report suggesting that autophagy is involved in mitochondrial dysfunction under SIRT1 knockdown,[17] I checked representative autophagy markers LC3-II and autophagosome in SiHa cells. Compared with Rapamycin, SIRT1 knockdown seldom induced autophagy based on the two parameters (Figures 8A and B). To summarize, SIRT1 contribute to the HPV-infected cervical cancers. SIRT1 knockdown is unlikely to induce cell death via apoptosis and necrosis, which may not be attributed to autophagy also.

## AIM2 inflammasome-related genes are upregulated by SIRT1 knockdown.

To investigate the role of SIRT1 in cervical cancer cells, I conducted cDNA microarray and performed DAVID functional annotation cluster analysis, as was summarized in Figure 9A. Immune and virus response-related gene sets were as highly ranked as those in response to SIRT1 knockdown (Figure 9B). The immune response-related genes induced by SIRT1 knockdown and the virus response-related genes are listed in Figure 10A. Among cell death-related genes (Figure 10B), AIM2 in the pyroptosis-related gene set was up-regulated to the highest extent (~42 fold) by SIRT1 knockdown. Therefore, AIM2-driven pyroptosis was first considered as a possible mechanism of cell death. Pyroptosis has distinct features, such as plasma membrane rupture, vacuole formation, ion channel imbalance, cytokine processing and release, cell swelling, DNA fragmentation, and mitochondrial damage.[18-21] Indeed, mitochondrial dysfunction, cell swelling, vacuolization, and calcium influx were observed in SIRT1-knocked-down cells, all of which are known to occur during pyroptosis. Heat map

analysis supports the activation of the AIM2 inflammasome signaling pathway in SIRT1-knocked-down SiHa cells (Figure 11A). In the TCGA database of cervical cancer, AIM2 and caspase-1 levels are higher in the low-SIRT1 group than in the high-SIRT1 group (Figure 11B). Gene set enrichment analysis also showed that AIM2 inflammasome-related genes were negatively regulated by SIRT1 (Figure 11C).

## SIRT1 knockdown causes diverse pyroptotic cell death phenomenon.

I have often observed that phenol red-containing media became yellowish in SIRT1-knocked-down SiHa cell culture (Figure 12A), prompting me to measure the pH. The acidification of media occurred faster in SIRT1-knocked-down SiHa cells than in control cells (Figure 12B). The intracellular levels of lactate and pyruvate were elevated by SIRT1 knockdown, whereas the ATP levels were significantly reduced (Figures 13A-C). These results strongly indicate that glucose energy metabolism is impaired by SIRT1 knockdown. When examined using an electron microscope (Figure 14A), mitochondria were reduced in number but became larger in

SIRT1-knocked-down cells (Figure 14B), which are typical features of less active respiration.[22,23] More surprisingly, the SIRT1-knocked-down cells were severely swollen with many vacuoles in the cytoplasm (Figures 14C and D). Because cell swelling reflects the breakdown of ionic homeostasis, I analyzed the intracellular calcium level and found that a substantial amount of $Ca^{2+}$ enters SIRT1-knocked-down cells (Figures 15A and B). Taken together, SIRT1 knockdown provokes metabolic and morphological changes in cervical cancer cells.

## SIRT1 knockdown induces cell death by activating the AIM2 inflammasome.

AIM2, which is known to drive pyroptosis through the inflammasomal pathway in response to DNA viruses, was found to be upregulated by SIRT1 knockdown (Figure 16A). The inflammasome mediator caspase-1 and its cleaved form p20 were also induced by silencing SIRT1 with either single siRNA or siPool (Figure 16B). Given that AIM2 knockdown rescued cell growth following SIRT1 knockdown, the AIM2 inflammasome might mediate SIRT1 knockdown-induced cell

death (Figure 16C). A caspase-1 inhibitor Ac-YVAD-cmk also rescued cell growth in SIRT1-knocked-down SiHa cells (Figure 17A). The specificity of Ac-YVAD-cmk to caspase-1 was confirmed by checking no effects of this compound on caspase-3 activation (Figures 17B and C). Downstream genes of the AIM2 inflammasome were upregulated by SIRT1 knockdown (Figure 18). The AIM2 induction by SIRT1 knockdown was reversed by SIRT1 restoration (Figures 19A and B). To examine whether SIRT1 controls the transcription of the *AIM2* gene, I measured the activity of the AIM2 promoter using an AIM2 promoter-luciferase fusion gene. The luciferase activity was enhanced by SIRT1 knockdown, an effect that was reversed by SIRT1 restoration (Figure 19C).

### SIRT1 knockdown increase RELB mRNA stability.

Using the LASAGNA-Search 2.0 program (http://biogrid-lasagna.engr.uconn.edu/lasagna_search/), I found putative binding segments of NF-κB (-562 to -549, 5′-GGGGAAATTCCCAC-3′) and STAT1 (-456 to -446, 5′-TTTCCCAGAAA-3′) at the *AIM2* promoter. In SIRT1-knocked-down SiHa cells, the level of AIM2 mRNA and

luciferase activity of the AIM2-luciferase reporter were both significantly reduced by co-knockdown of RelB (Figures 20A and B). In addition, when a part of the putative NF-κB binding segment was mutated, AIM2 promoter activity was no longer regulated by SIRT1 knockdown (Figure 20C), further supporting the involvement of NF-κB in AIM2 transcription. I performed ChIP assay to examine whether RelB acts as the transcription factor for the *AIM2* gene. The RelB binding to the AIM2 promoter was profoundly enhanced by SIRT1 knockdown (Figure 20D). Moreover, the nuclear level of RelB was increased by SIRT1 knockdown (Figure 21A). Since the SIRT1 knockdown increased the amount of RelB protein even in cell lysates and the cytoplasmic fraction, the RelB upregulation may be the primary cause for the AIM2 induction by SIRT1 knockdown. To understand how SIRT1 controls RelB expression, I first measured the levels of RELB mRNA and its pre-mRNA (for checking de novo transcription). Given that the RelB pre-mRNA level was not changed by SIRT1 knockdown, RelB mRNA expression may be upregulated at the post-transcriptional level (Figure 21B). However, the degradation of RELB mRNA was significantly blocked by SIRT1 knockdown

(Figure 21C), suggesting that SIRT1 negatively regulates the stability of AIM2 mRNA. Collectively, SIRT1 is likely to protect cervical cancer cells from pyroptotic cell death by suppressing the NF-kB-mediated AIM2 expression via destabilization of RelB mRNA.

## SIRT1 promotes cervical cancer cell survival in a deacetylase-independent manner.

To confirm the SIRT1 function of deacetylase, I expressed wild-type SIRT1_ORF (open reading frame) or its deacetylase-defective mutants into SiHa cells, where endogenous SIRT1 was silenced using an siRNA targeting the 3′-UTR of *SIRT1* mRNA (Figure 22A). Unexpectedly, mutated SIRT1s, as well as wild-type SIRT1, could rescue the proliferation of SIRT1-knocked-down cells (Figure 22B). Moreover, three SIRT1 inhibitors, even at effective concentrations (Figure 23A), failed to reduce cell growth (Figure 23B). These results suggest that SIRT1 promotes SiHa cell proliferation irrespectively of its deacetylase activity.

## AIM2 inflammasome-mediated pyroptosis is intercellularly

transmitted.

In contrast to apoptotic cells dying silently, pyroptotic cells announce the death to neighboring cells by secreting proinflammatory cytokines and releasing cellular contents.[24,25] Despite limited transfection, a large population of cervical cancer cells died following siRNA exposure. This discrepancy encouraged me to hypothesize that cell death could be spread out. Strikingly, the growth of healthy SiHa cells (RFP-labeled) was noticeably reduced by co-culture with pyroptotic SiHa cells (GFP-labeled, SIRT1-knocked-down) (Figure 24A). I collected culture media from pyroptotic cells and treated with the conditioned media. The conditioned media from pyroptotic cells inhibited cell growth in naïve cervical cancer cell lines (Figure 24B). Interestingly, this phenomenon was also observed in HeLa cells, which showed no response to SIRT1 knockdown. In addition, cell growth retardation by the conditioned medium was reversed by Ac-YVAD-cmk (Figure 25A). Also, most pyroptotic events were induced in SiHa cells exposed to the conditioned medium - that is, AIM2 induction, caspase-1 activation (Figure 25B), cell swelling, cytoplasmic vacuolization, mitochondrial reduction (Figures 26A and B), and

calcium influx (Figure 27). Accordingly, SiHa cells undergoing pyroptotic death seem to release some factor(s) that kill neighboring cancer cells through AIM2 inflammasome-mediated pyroptosis.

## The AIM2 inflammasome is transmitted through extracellular vesicles.

To estimate the molecular weight of pyroptosis-transmitting factor, I passed the SiHa-conditioned medium through a 100-kDa cut-off membrane (Figure 28A). The retentate effectively inhibited proliferation in naïve SiHa cells, but the permeate did not (Figure 28B). Given that the anti-proliferative activity of the retentate was abolished by brief boiling, the bioactive factor may be a heat-denaturable molecule like a polypeptide (Figure 28C). However, considering that most peptide-based cytokines in monomeric states are less than 100 kDa, I considered two possibilities concerning the pyroptosis-transmitting factor: it forms a multimeric complex, or it is included in a big parcel. Given that many extracellular vesicles are released from SIRT1-knocked-down SiHa cells on EM images (Figure 14A), I decided to check the latter case. The EM images showed that

extracellular vesicles were enriched in the SIRT1-knocked-down SiHa-conditioned medium at the final step for vesicle isolation (Figure 29A). The question arises regarding whether cytoplasmic proteins can be transferred to recipient cells. To this end, I used a stable SiHa cell line expressing GFP. GFP was identified in purified extracellular vehicles, and its content was higher in extracellular vesicles from SIRT1-knocked-down cells (si-SIRT1_EV) (Figure 29B). In addition, GFP expressed in SIRT1-knocked-down cells can be transferred into naïve cells, as demonstrated by Western blotting (Figure 29B) and flow cytometry (Figure 29C). Given that recipient cells also underwent pyroptotic death, I examined whether the AIM2 inflammasome is included within extracellular vesicles. Compared with si-Cont_EV, si-SIRT1_EV included AIM2 and caspase-1 at higher levels and inhibited the proliferation of recipient cells (Figures 29D and 30A). CD63 and HSP70 were analyzed as representative exosome markers. In the recipient cells exposed to si-SIRT1_EV, AIM2 and caspase-1 levels were substantially increased (Figure 30B). Overall, these results further support our notion that inflammasome-mediated pyroptosis is propagated via extracellular vesicles.

## The SIRT1-AIM2 axis is a potential target for cervical cancer therapy.

To evaluate whether the SIRT1-AIM2 axis could be an emerging target for cervical cancer therapy, two sets of xenograft studies were designed. I injected si-SIRT1 RNA or si-SIRT1_EV into cervical cancer xenografts (Figure 31A). Either si-SIRT1 or si-SIRT1_EV injection reduced tumor growth rates (Figures 31B and C) and tumor weights (Figures 32A) without any significant change in body weight (Figures 32B). AIM2, caspase-1, caspase-1 p20, and CD63 expression levels were increased in tumor tissues treated with either si-SIRT1 or si-SIRT1_EV (Figures 33A and B). In immunohistochemical analyses, the upregulation of these inflammasome markers was overtly demonstrated (Figure 34 and Figure 35). In EM images, many cells in the tumors treated with si-SIRT1 were severely vacuolated, as shown in cultured cells treated with si-SIRT1 (Figure 36).

## SIRT1 expression correlates with poor clinical outcome in cervical cancer.

Next, I investigated whether SIRT1 expression is associated with the survival outcomes of cervical cancer patients. I analyzed SIRT1 expression by immunohistochemical analysis in human cervical cancer tissue arrays (Figure 37A) and divided patients into two groups, SIRT1_high and _low, based on the median value (Figure 37B). Age, sex, and staging at diagnosis were not statistically different between the high and low groups. Thus, a high expression of SIRT1 was associated with poor survival in the cervical cancer population (Figure 37C). In addition, AIM2 and caspase-1 p20 levels were significantly lower in the SIRT1_high group than in the SIRT1_low group (Figure 38A) and were also inversely correlated with SIRT1 expression (Figure 38B). Thus, SIRT1 overexpression seems to promote the growth and progression of cervical cancer by blocking AIM2 inflammasome-mediated cell death.

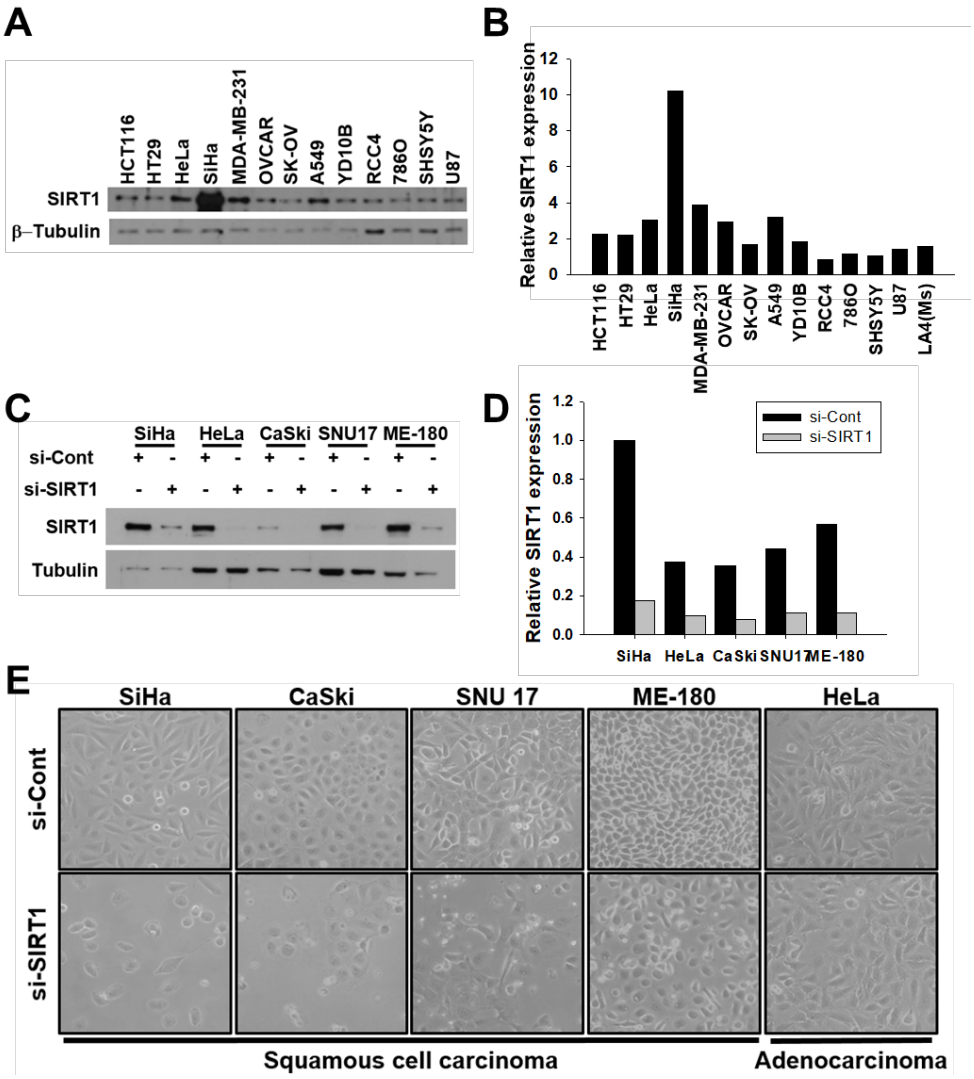
A
HCT116
HT29
HeLa
SiHa
MDA-MB-231
OVCAR
SK-OV
A549
YD10B
RCC4
786O
SHSY5Y
U87
SIRT1
β–Tubulin
B
Relative SIRT1 expression
0
2
4
6
8
10
12
HCT116
HT29
HeLa
SiHa
MDA-MB-231
OVCAR
SK-OV
A549
YD10B
RCC4
786O
SHSY5Y
U87
LA4(Ms)
C
SiHa
HeLa
CaSki
SNU17
ME-180
si-Cont
si-SIRT1
SIRT1
Tubulin
D
Relative SIRT1 expression
0.0
0.2
0.4
0.6
0.8
1.0
1.2
si-Cont
si-SIRT1
SiHa
HeLa
CaSki
SNU17
ME-180
E
SiHa
CaSki
SNU 17
ME-180
HeLa
si-Cont
si-SIRT1
Squamous cell carcinoma
Adenocarcinoma

Figure 1. SIRT1 is vital for cell survival in cervical cancer.

(A) Western blot analyses of SIRT1 and β-tubulin in various cancer cell lines. (B) Bar graph represents relative SIRT1 expression in various cancer cell lines. (C) Western blot analysis of SIRT1 in cancer cells transfected with siRNAs. (D) Bar graph represents relative SIRT1 expression in cervical cancer cell lines. (E) Cells ($5\times10^5$/well) were seeded in 6-well plates, and transfected with non-targeting or SIRT1-targeting siRNAs (40 nM).

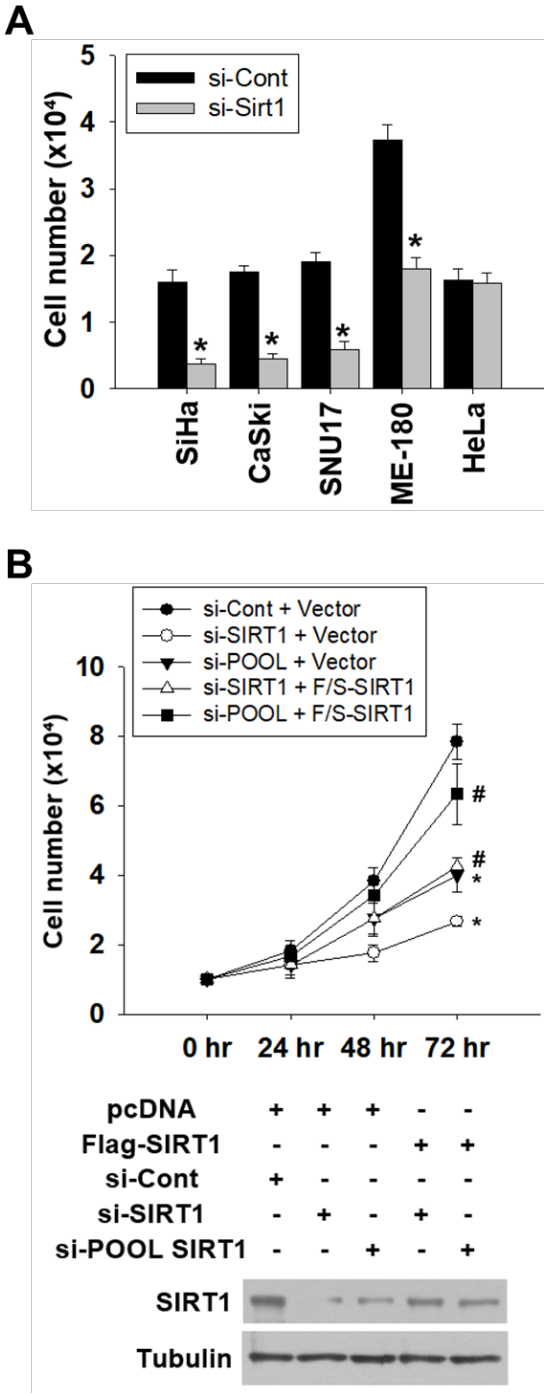
A
si-Cont
si-Sirt1
Cell number (x10⁴)
0
1
2
3
4
5
*
SiHa
CaSki
SNU17
ME-180
HeLa
B
si-Cont + Vector
si-SIRT1 + Vector
si-POOL + Vector
si-SIRT1 + F/S-SIRT1
si-POOL + F/S-SIRT1
Cell number (x10⁴)
0
2
4
6
8
10
#
*
0 hr
24 hr
48 hr
72 hr
pcDNA + + + - -
Flag-SIRT1 - - - + +
si-Cont + - - - -
si-SIRT1 - + - + -
si-POOL SIRT1 - - + - +
SIRT1
Tubulin

**Figure 2. Effects of SIRT1 knockdown on cervical cancer cell growth.**

(A) Cervical cancer cells were transfected with 40 nM siRNAs, incubated for 72 hours, and counted using a hemocytometer. Each bar represents the mean + SD from 4 separate experiments. * denotes $P < 0.05$ (Student's t test) versus the si-Cont group. (B) SiHa cells, which had been co-transfected with the indicated siRNA and plasmid, were cultured for 1-3 days, and counted. Each point represents the mean + SD (n=4). *, $P < 0.05$ versus the si-Cont/Vector group; #, $P < 0.05$ versus the si-SIRT1/Vector group or si-POOL/Vector group. *, # $P < 0.05$ by Student's t test.

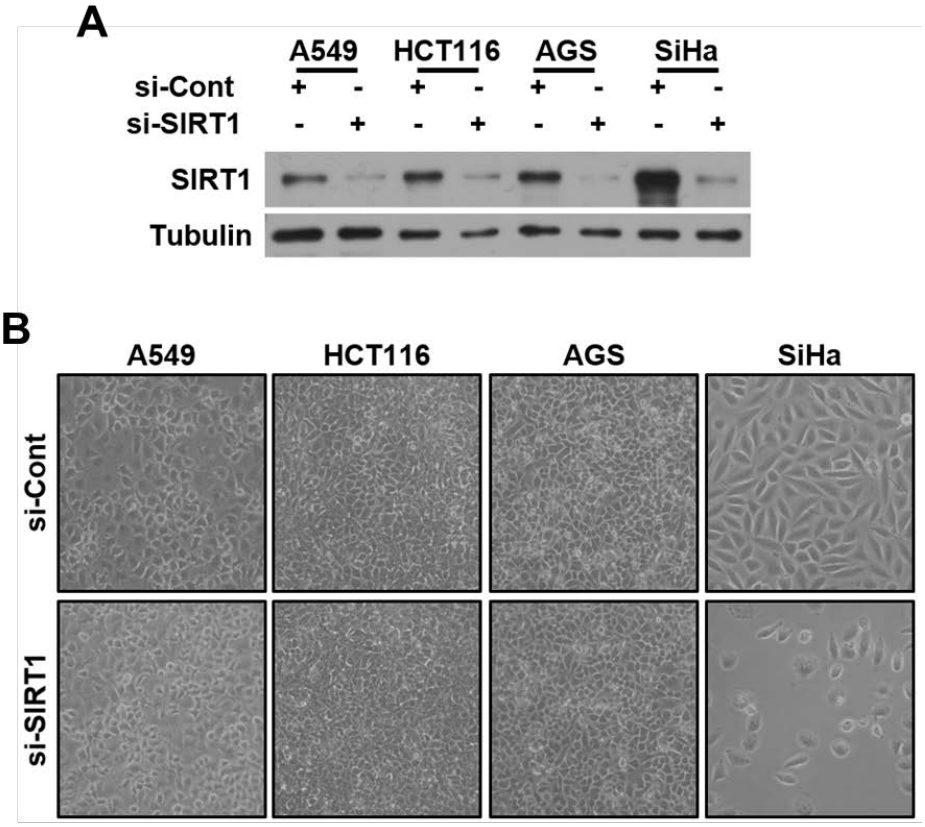
A
A549
HCT116
AGS
SiHa
si-Cont
si-SIRT1
SIRT1
Tubulin
B
A549
HCT116
AGS
SiHa
si-Cont
si-SIRT1
C
si-Cont
si-SIRT1
Relative Cell number
1.4
1.2
1.0
0.8
0.6
0.4
0.2
0.0
*
A549
HCT116
AGS
SiHa

**Figure 3. Effects of SIRT1 knockdown on several cancer cells growth.**

(A) Cancer cells were seeded at $5\times10^5$ cells/well in 6-well plates, transfected with 40 nM siRNA, and incubated for 48 hours. SIRT1 knock-down was verified by immunoblotting. (B) Cell density and shape were checked by photography. (C) Diverse cancer cells were transfected with 40 nM siRNAs, incubated for 72 hours, and counted using a hemocytometer. Each bar represents the mean + SD from 4 separate experiments. * denotes $P < 0.05$ (Student's t test) versus the si-Cont group.

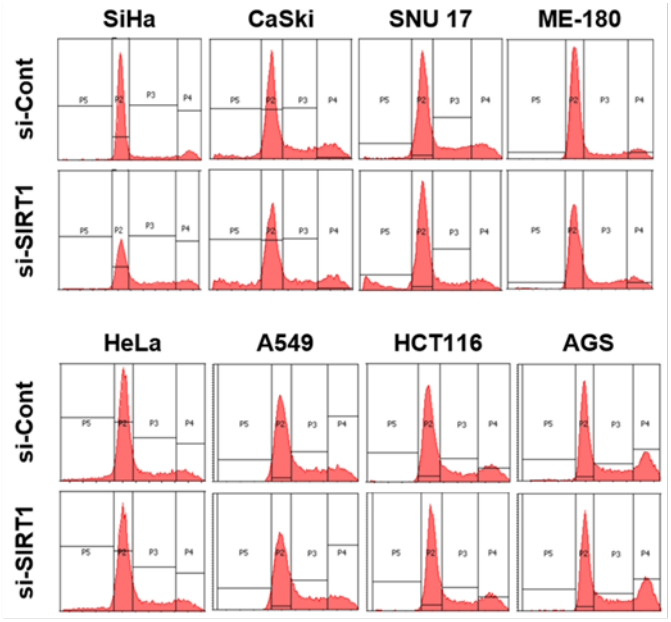
SiHa
CaSki
SNU 17
ME-180
si-Cont
si-SIRT1
HeLa
A549
HCT116
AGS
si-Cont
si-SIRT1

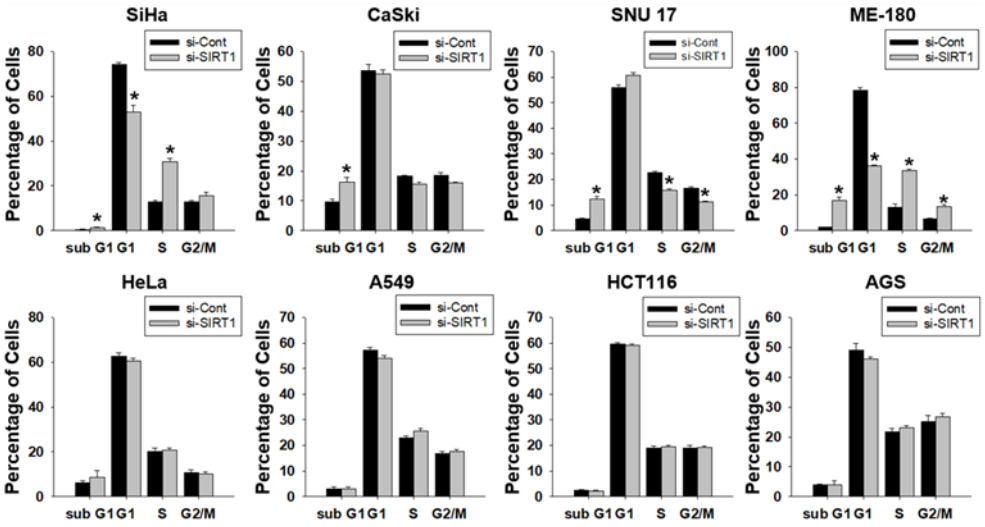
SiHa
CaSki
SNU 17
ME-180
HeLa
A549
HCT116
AGS
si-Cont
si-SIRT1
Percentage of Cells
sub G1
G1
S
G2/M

Figure 4. Cell cycle analyses in cervical cancer cell.

The top panels represent histograms of DNA contents in cancer cells which had been transfected with siRNAs and incubated for 48 hours. The bottom panels represent the bar graphs of cell cycle analyses (the means ± SD, n=4). *P < 0.05 versus the si-Cont group by Mann-Whitney U test.

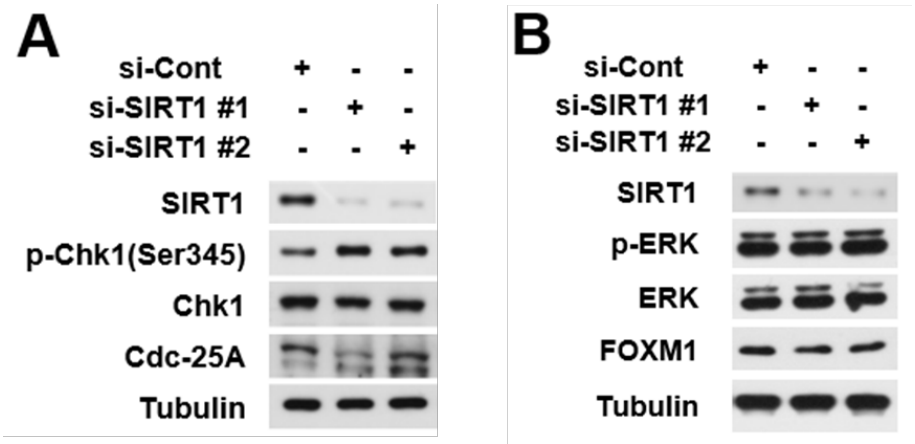


Figure 5. Cell cycle pathway study in SIRT1 knockdown cells.

(A) and (B) SiHa cells were seeded at $5\times10^5$ cells/well in 6-well plates, transfected with 40 nM siRNA, and incubated for 48 hours.

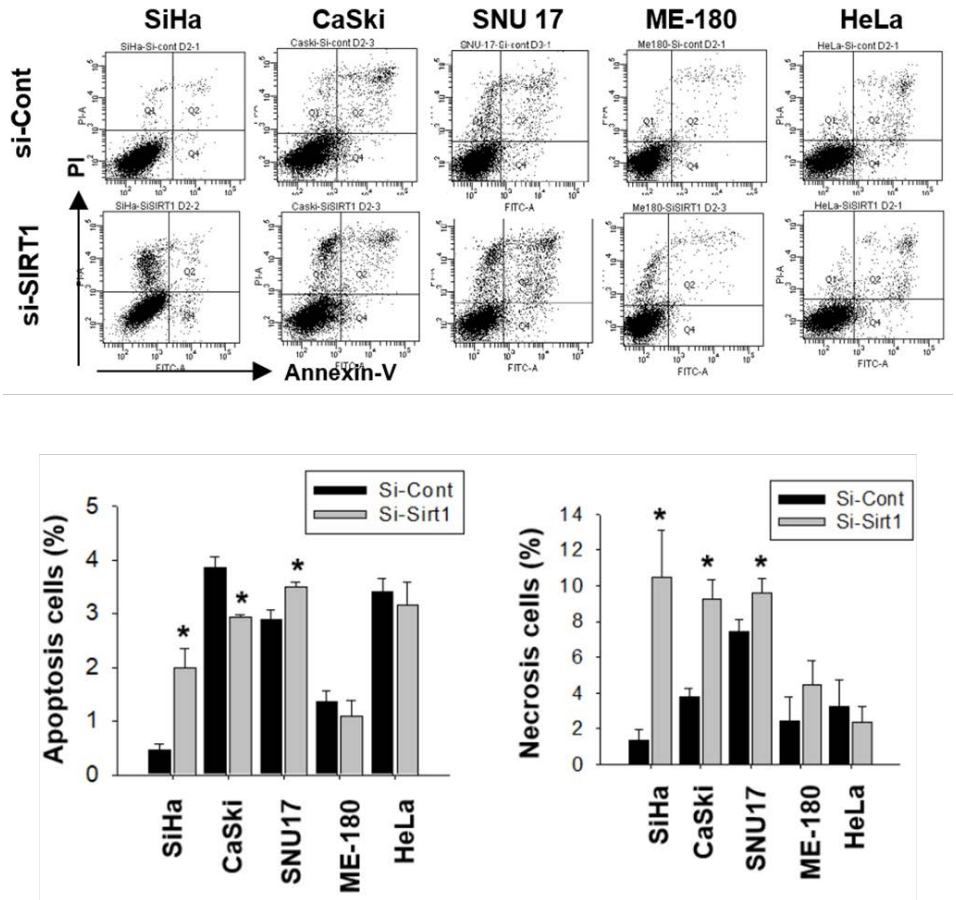


Figure 6. Cell death analyses in cervical cancer cell.

Various cervical cancer cell lines were transfected with siRNAs and incubated for 2 days. Cells were stained with annexin V and propidiium iodide and subjected to flow cytometric analysis. Cells in the right lower quadrant and the left upper quadrant windows were counted as apoptotic and necrotic cells, respectively. Each bar represents the mean ± SD of cell population (n=4). *P < 0.05 versus the si-Cont group by Student's t test.

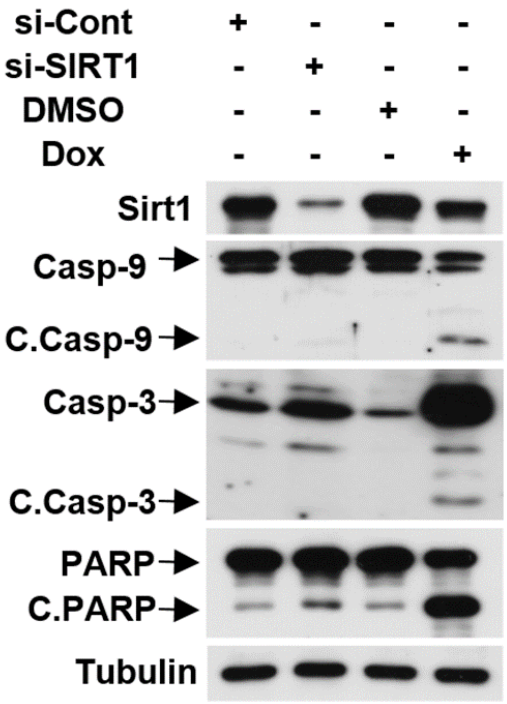


Figure 7. SIRT1 knockdown induces non-apoptotic cell death in cervical cancer cell.

Apoptosis markers were immunoblotted in SiHa cells transfected and incubated for 2 days. Doxorubicin was used as a positive control to verify apoptosis.

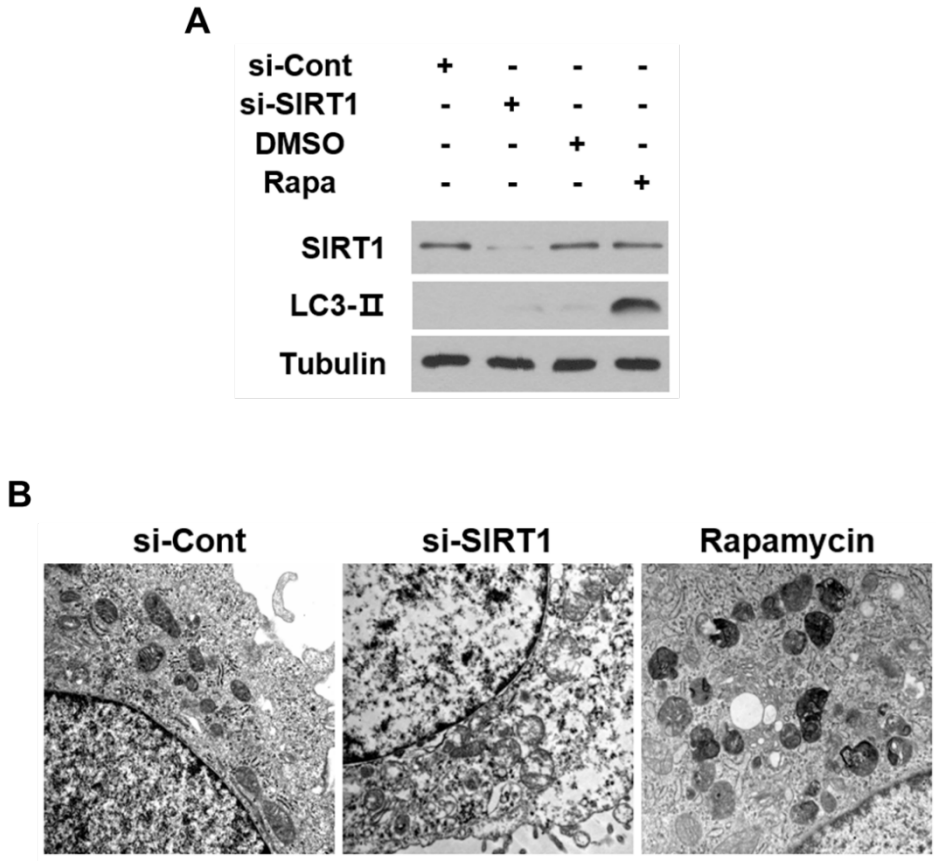


Figure 8. SIRT1 knockdown induces cervical cancer cell damage in an autophagy independent-manner.

(A) Autophagy markers were immunoblotted in SiHa cells transfected and incubated for 2 days. Rapamycin (10 μM) was used as a positive control to verify autophagy. (B) Transfected or rapamycin treated SiHa cells were incubated for 48 hours, fixed, and photographed on TEM.

A

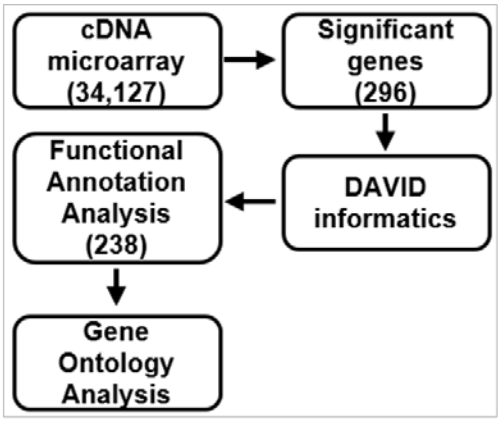
cDNA microarray (34,127)
Significant genes (296)
DAVID informatics
Functional Annotation Analysis (238)
Gene Ontology Analysis

B

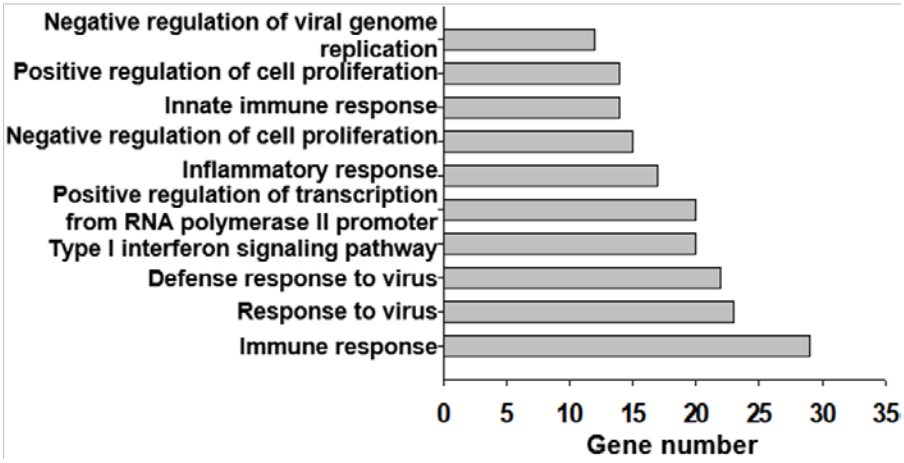
Negative regulation of viral genome replication
Positive regulation of cell proliferation
Innate immune response
Negative regulation of cell proliferation
Inflammatory response
Positive regulation of transcription from RNA polymerase II promoter
Type I interferon signaling pathway
Defense response to virus
Response to virus
Immune response
0
5
10
15
20
25
30
35
Gene number

**Figure 9. cDNA microarray analysis of the SIRT1 knockdown in cervical cancer cell.**

(A) Schematic flow chart for DAVID Gene Ontology Analysis of cDNA microarray. (B) DAVID Functional Annotation Clustering analysis of cDNA microarray. SiHa cells were transfected with 40 nM si-Cont or si-SIRT1 RNA, incubated for 24 h, and prepared for RNA isolation. The cDNA microarray analyses were performed in triplicate. The bar chart depicts the major biological pathways of gene sets that were upregulated over 5-fold in SIRT1 knocked down cells than in the control cells.

**A**

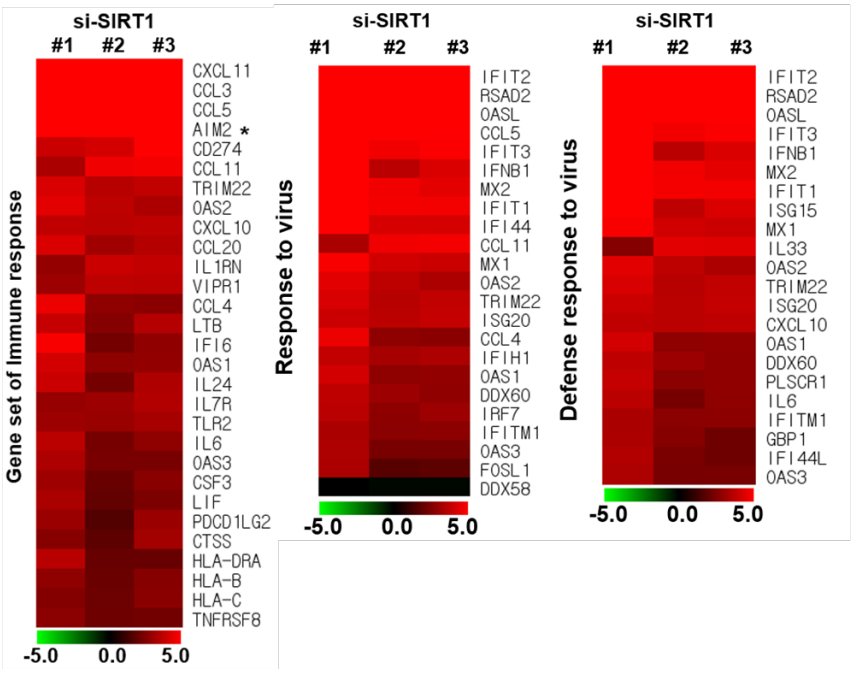


**B**

| Rank | Apoptosis (163) | | Necrosis (64) | | Autophagy (73) | | Necroptosis (57) | | Pyroptosis (26) | |
|---|---|---|---|---|---|---|---|---|---|---|
| | Gene | Fold | Gene | Fold | Gene | Fold | Gene | Fold | Gene | Fold |
| 1 | CD38 | 29 | TNFRSF8 | 5.3 | TRIM22 | 14.9 | IFNB1 | 28.4 | AIM2 | 42.3 |
| 2 | IFNB1 | 28.4 | TNFAIP3 | 4.5 | TRIM21 | 3.9 | C6 | 19.7 | GSDMC | 22.3 |
| 3 | ISG20 | 14.4 | TNFRSF6B | 3.9 | ADRB2 | 2.4 | IL1A | 10.5 | CTSG | 14.6 |
| 4 | PLAT | 12.7 | TNFRSF11A | 3.9 | MID2 | 2.2 | TNF | 3.6 | GBP1 | 6.7 |
| 5 | IL1A | 10.5 | TNFRSF9 | 3.7 | PLEKHF1 | 2 | TNFRSF21 | 3.4 | IL1B | 4.4 |

**Figure 10. Heatmap analyses of the significant gene sets in SIRT1 knockdown.**

(A) Heatmap analysis of the significant gene sets using the Multiple Experiment Viewer software. The relative level of a gene in each row was normalized to the mean value in the si-Control group by $\log_2$ transformation. The color scale represents expression values; green for low expression and red for high expression. (B) The tables list top five-ranked genes in cell death-elated gene sets.

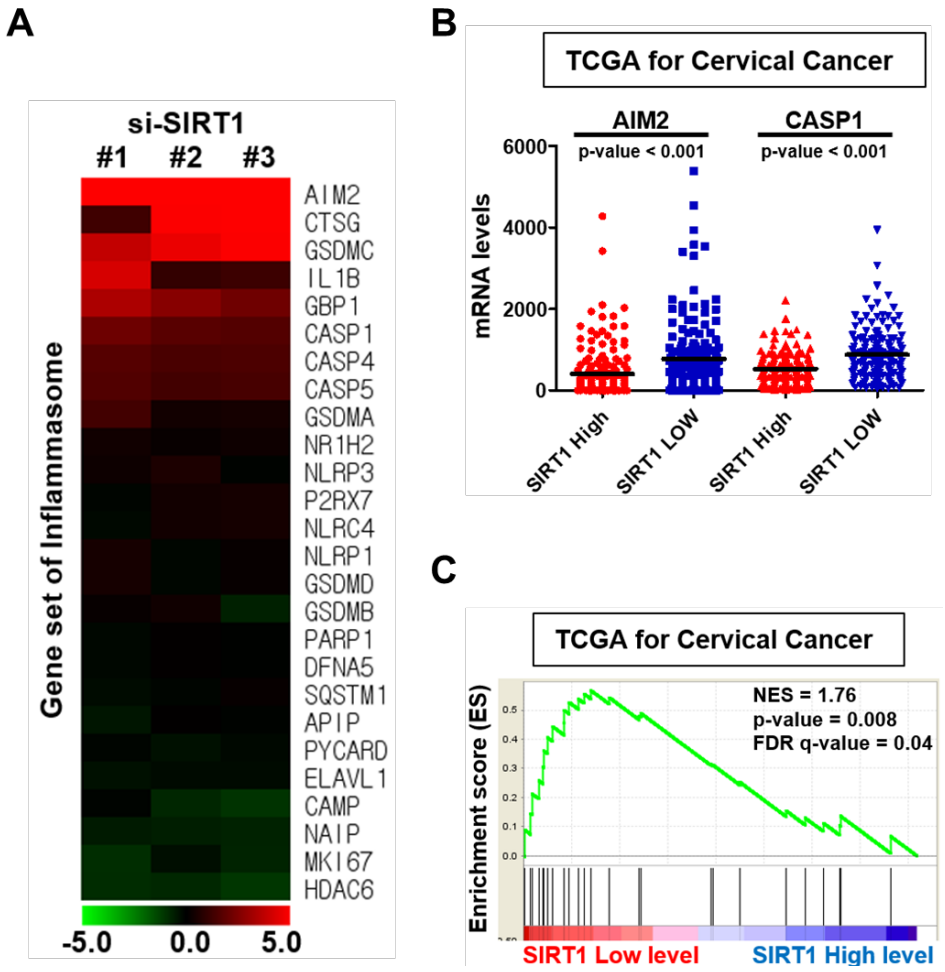
A
si-SIRT1
#1 #2 #3
Gene set of Inflammasome
AIM2
CTSG
GSDMC
IL1B
GBP1
CASP1
CASP4
CASP5
GSDMA
NR1H2
NLRP3
P2RX7
NLRC4
NLRP1
GSDMD
GSDMB
PARP1
DFNA5
SQSTM1
APIP
PYCARD
ELAVL1
CAMP
NAIP
MKI67
HDAC6
-5.0 0.0 5.0
B
TCGA for Cervical Cancer
AIM2
p-value < 0.001
CASP1
p-value < 0.001
mRNA levels
6000
4000
2000
0
SIRT1 High
SIRT1 LOW
SIRT1 High
SIRT1 LOW
C
TCGA for Cervical Cancer
Enrichment score (ES)
NES = 1.76
p-value = 0.008
FDR q-value = 0.04
SIRT1 Low level
SIRT1 High level

**Figure 11. Negative correlation between SIRT1 and AIM2 in cervical cancer.**

(A) Heatmap analysis of the AIM2/inflammasome-related gene set. (B) The mRNA levels of AIM2 and CASP1 in SIRT1_High and SIRT1_Low groups of cervical cancer on TCGA. Horizontal bars represent the mean values of AIM2 or CASP1, and the p values were calculated by Mann-Whitney U test. (C) Gene set enrichment analysis (GSEA) between SIRT1 and the AIM2/inflammasome-related gene set. The data sets, derived from tumor tissues of cervical cancer patients, were imported from The Cancer Genome Atlas (NIH, TCGA) and divided into two groups depending on SIRT1 mRNA expression levels.

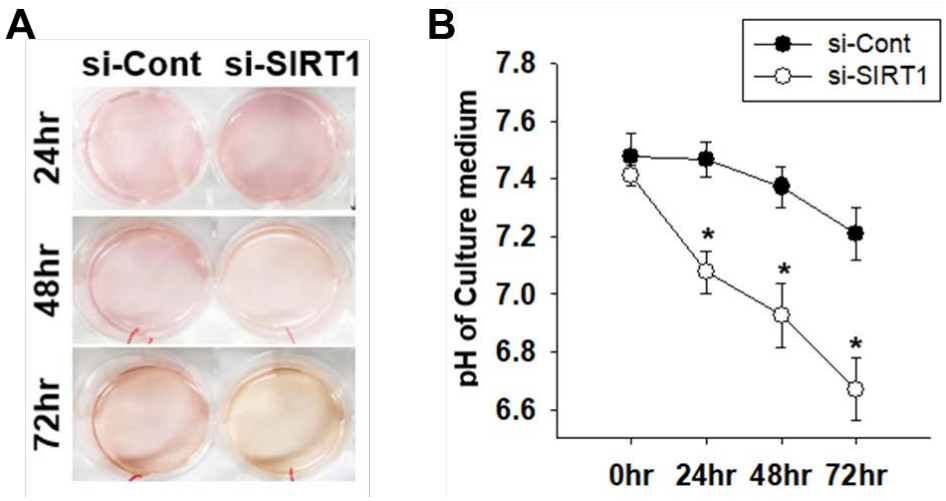


Figure 12. The acidification of media occurred faster in SIRT1 knockdown cell.

(A) SiHa cells were seeded at $5\times10^5$ cells/well in 6-well plates, transfected with siRNAs, and incubated for 1-3 days. The culture dishes were photographed. (B) The pH was measured in the culture media for SiHa cells transfected with siRNAs. Each point represents the mean ± SD (n=4). *P < 0.05 versus the si-Cont group by Student's t test.

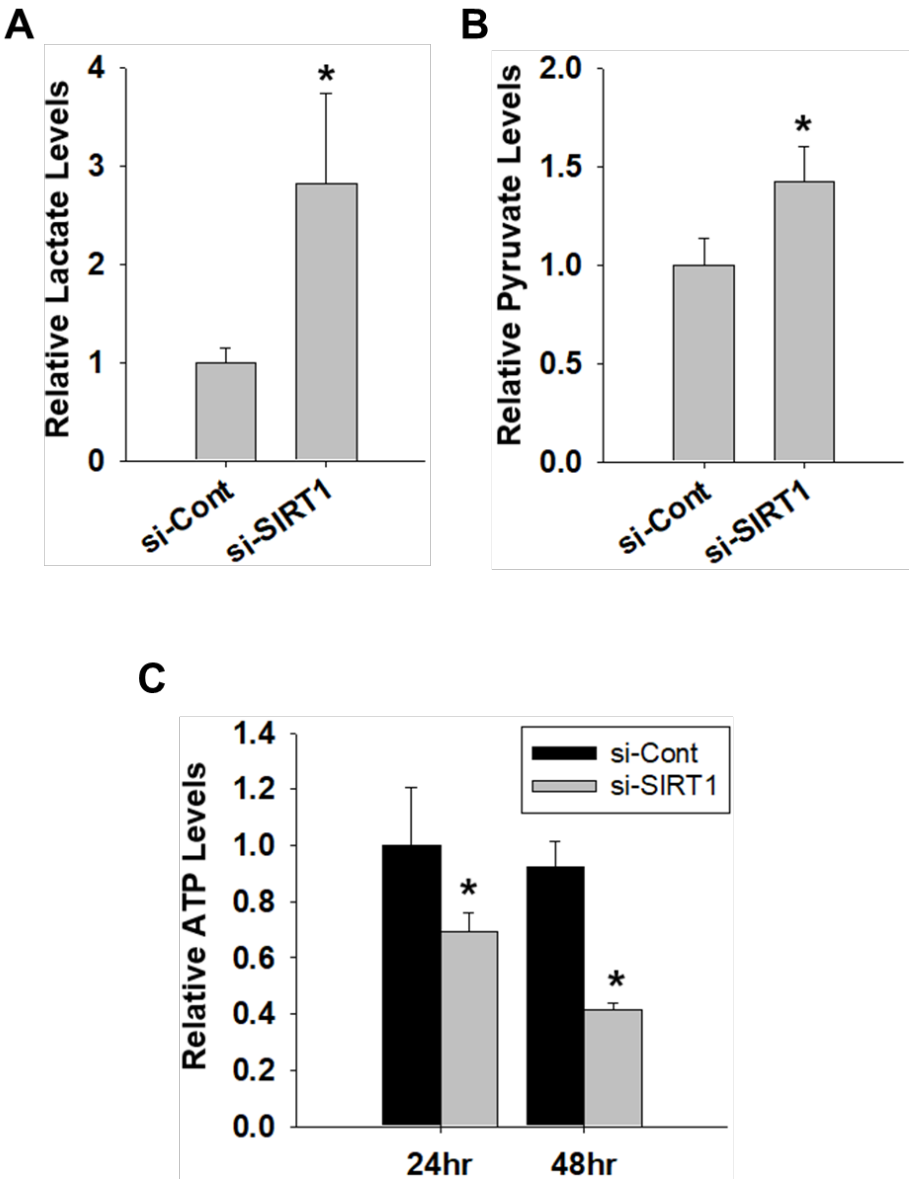
A
Relative Lactate Levels
4
3
2
1
0
*
si-Cont
si-SIRT1
B
Relative Pyruvate Levels
2.0
1.5
1.0
0.5
0.0
*
si-Cont
si-SIRT1
C
Relative ATP Levels
1.4
1.2
1.0
0.8
0.6
0.4
0.2
0.0
si-Cont
si-SIRT1
*
*
24hr
48hr

**Figure 13. Effects of SIRT1 knockdown on glucose energy metabolism in cervical cancer cell.**

(A–C) The levels of intracellular lactate, pyruvate, and ATP were measured as described in Supplementary Methods. Transfected SiHa cells were incubated for 48 hours. Each bar represents the mean + SD (n=4). *P < 0.05 versus the si–Cont group by Student's t test.

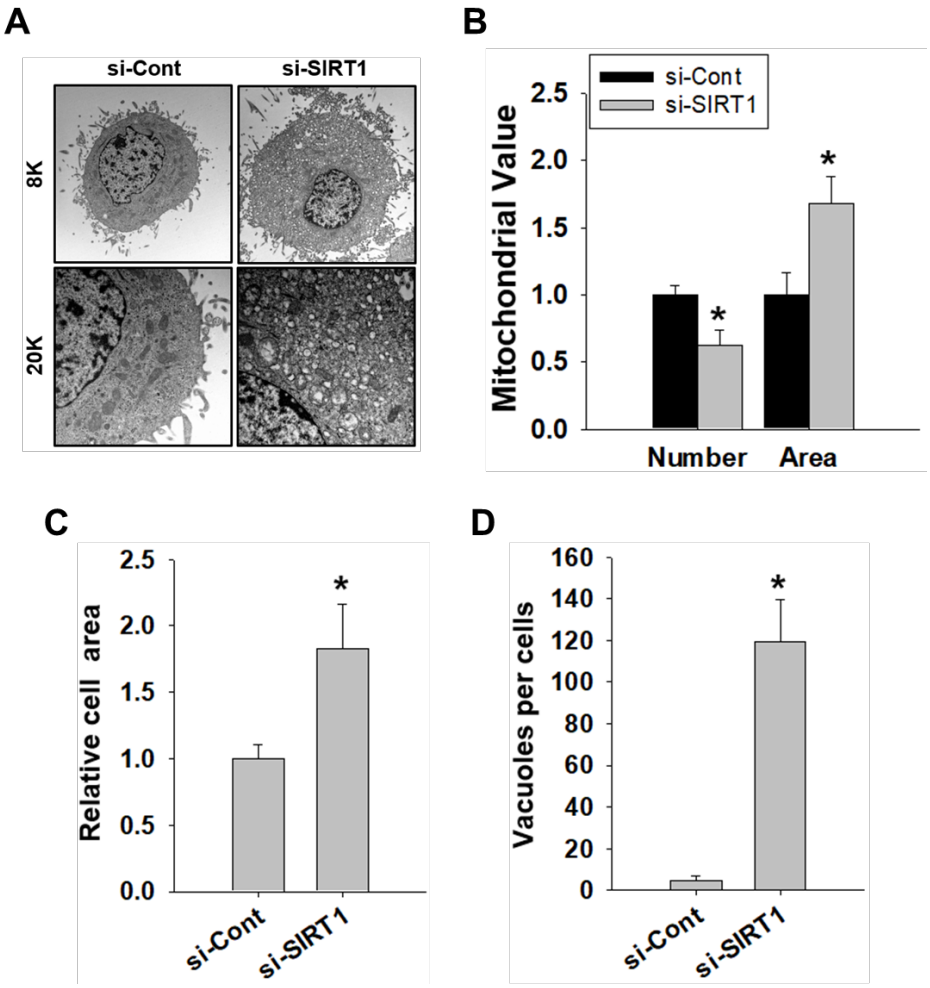
A
si-Cont
si-SIRT1
8K
20K
B
si-Cont
si-SIRT1
Mitochondrial Value
2.5
2.0
1.5
1.0
0.5
0.0
*
*
Number
Area
C
Relative cell area
2.5
2.0
1.5
1.0
0.5
0.0
*
si-Cont
si-SIRT1
D
Vacuoles per cells
160
140
120
100
80
60
40
20
0
*
si-Cont
si-SIRT1

Figure 14. SIRT1 knockdown provokes morphological changes in cervical cancer cell.

(A) Transfected SiHa cells were incubated for 48 hours, fixed, and photographed on TEM (x8,000 or x20,000 magnification). (B–D) Based on the TEM images, the number and area of mitochondria, cell area, and the number of intracellular vacuoles were measured using the ImageJ software. Each bar represents the mean + SD from 12 photographs in each group. *P < 0.05 versus the si–Cont group by Student's t test.

A

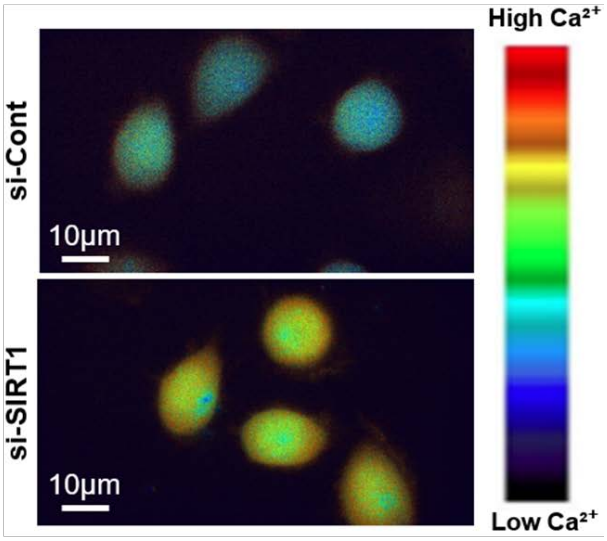
High Ca²⁺
si-Cont
10μm
si-SIRT1
10μm
Low Ca²⁺

B

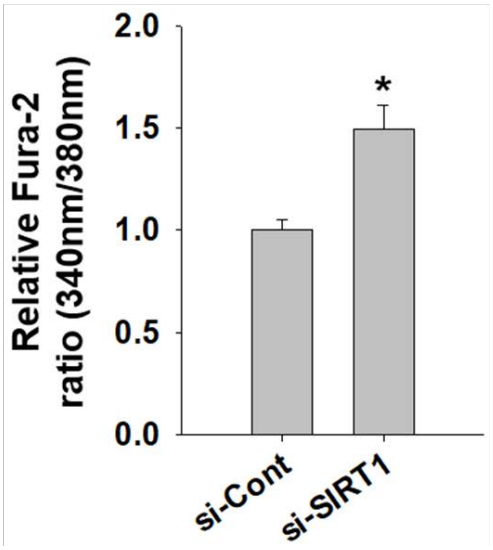
Relative Fura-2 ratio (340nm/380nm)
2.0
1.5
1.0
0.5
0.0
*
si-Cont
si-SIRT1

**Figure 15. SIRT1 knockdown causes an imbalance of the ionic homeostasis.**

(A) SiHa cells, which had been transfected with siRNAs, were cultured for 48 hours. Cells were incubated with 1 μM Fura-2 and photographed under a fluorescence microscope. (B) SiHa cells, which had been transfected with 40 nM siRNAs, were cultured for 48 hours. Cells were incubated with 1 μM Fura-2 and photographed under a fluorescence microscope. The ratio of fluorescence intensities at the excitation wavelengths 340 and 380 nm was measured to quantify intracellular calcium levels. Each bar represents the mean + SD from 20 independent experiments. *$P < 0.05$ versus the si-Cont group by Mann-Whitney U test.

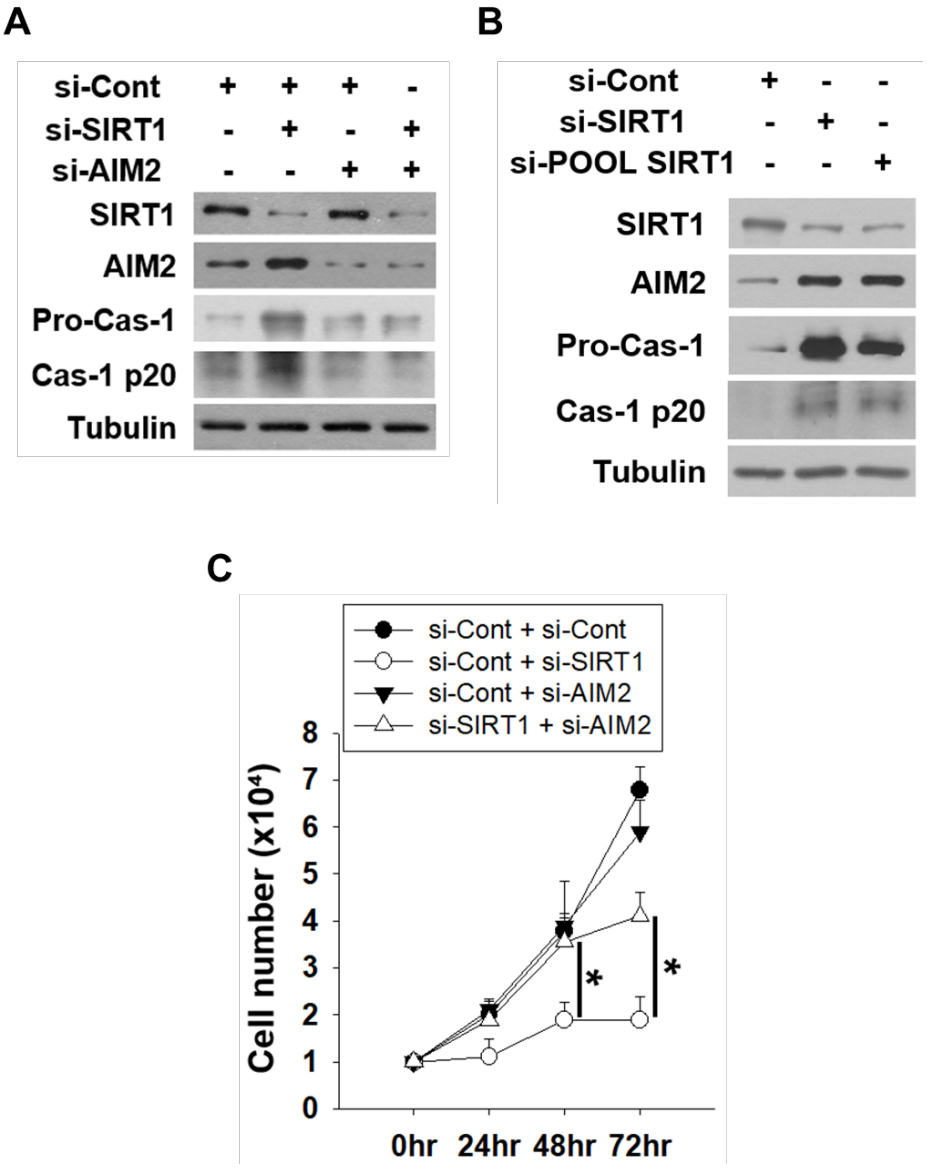
A
si-Cont + + + -
si-SIRT1 - + - +
si-AIM2 - - + +
SIRT1
AIM2
Pro-Cas-1
Cas-1 p20
Tubulin
B
si-Cont + - -
si-SIRT1 - + -
si-POOL SIRT1 - - +
SIRT1
AIM2
Pro-Cas-1
Cas-1 p20
Tubulin
C
si-Cont + si-Cont
si-Cont + si-SIRT1
si-Cont + si-AIM2
si-SIRT1 + si-AIM2
Cell number (x10⁴)
0
1
2
3
4
5
6
7
8
0hr 24hr 48hr 72hr
*
*

Figure 16. SIRT1 knockdown leads to cell death by activating the AIM2 inflammasome.

(A) SiHa cells were transfected with the indicated siRNAs (60 nM each), and 48 hours later lysed for Western blot analyses of AIM2 inflammasome-related proteins. (B) SiHa cells were transfected with the indicated siRNAs (40 nM each), and 48 hours later lysed for Western blot analyses of AIM2 inflammasome-related proteins. (C) SiHa cells were transfected with the indicated siRNAs, and counted. *P < 0.05 versus the si-Cont group by Student's t test.

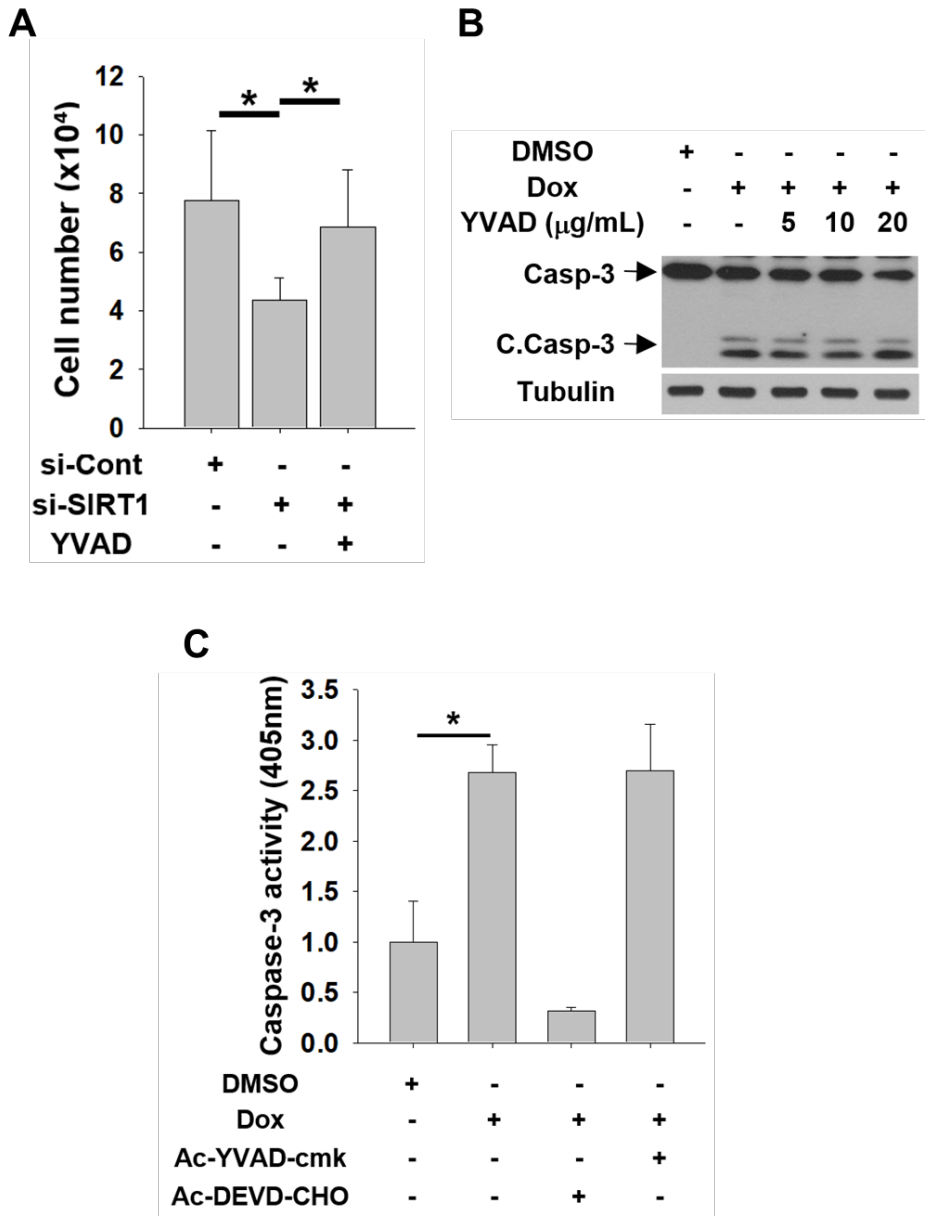
A
Cell number (x10⁴)
12
10
8
6
4
2
0
*
*
si-Cont + - -
si-SIRT1 - + +
YVAD - - +
B
DMSO + - - - -
Dox - + + + +
YVAD (μg/mL) - - 5 10 20
Casp-3
C.Casp-3
Tubulin
C
Caspase-3 activity (405nm)
3.5
3.0
2.5
2.0
1.5
1.0
0.5
0.0
*
DMSO + - - -
Dox - + + +
Ac-YVAD-cmk - - - +
Ac-DEVD-CHO - - + -

**Figure 17. Caspase-1 inhibitor rescues cell growth in SIRT1 knockdown cancer cell.**

(A) The transfected SiHa cells were treated with DMSO or Ac-YVAD-cmk (10 μg/mL), and counted on day 3. *P < 0.05 by Student's t test. (B) SiHa cells at $5\times10^5$/35-mm dish were treated with doxorubicin (5 μM) or/and Ac-YVAD-cmk for 24 hours. Caspase-3 and its cleaved form were detected by Western blotting. (C) SiHa cells were treated with doxorubicin (5 μM), Ac-DEVD-CHO (10 μM), or/and Ac-YVAD-cmk (10 μg/mL) for 12 hours, and lysed for caspase-3 activity assay. Each bar represents the mean ± SD (n=4). *P < 0.05 versus the DMSO by Student's t test.

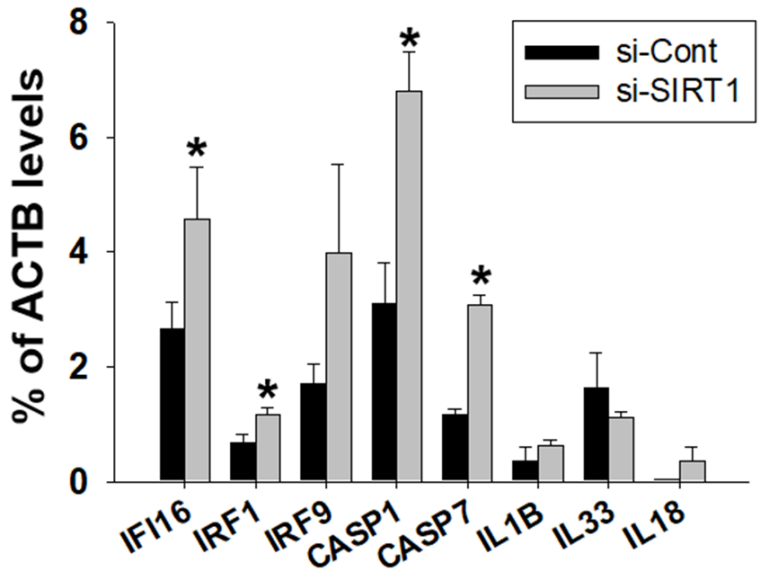


Figure 18. Downstream genes of the AIM2 inflammasome.

SiHa cells were transfected with the siRNA and incubated for 24 hours. The mRNAs were subjected to cDNA microarray analyses. Bars represent the relative mRNA levels (means + SD, n = 3) of AIM2 inflammsome-related genes, whose levels were normalized to β-actin (*ACTB*). *, $P < 0.05$ by Student's t test.

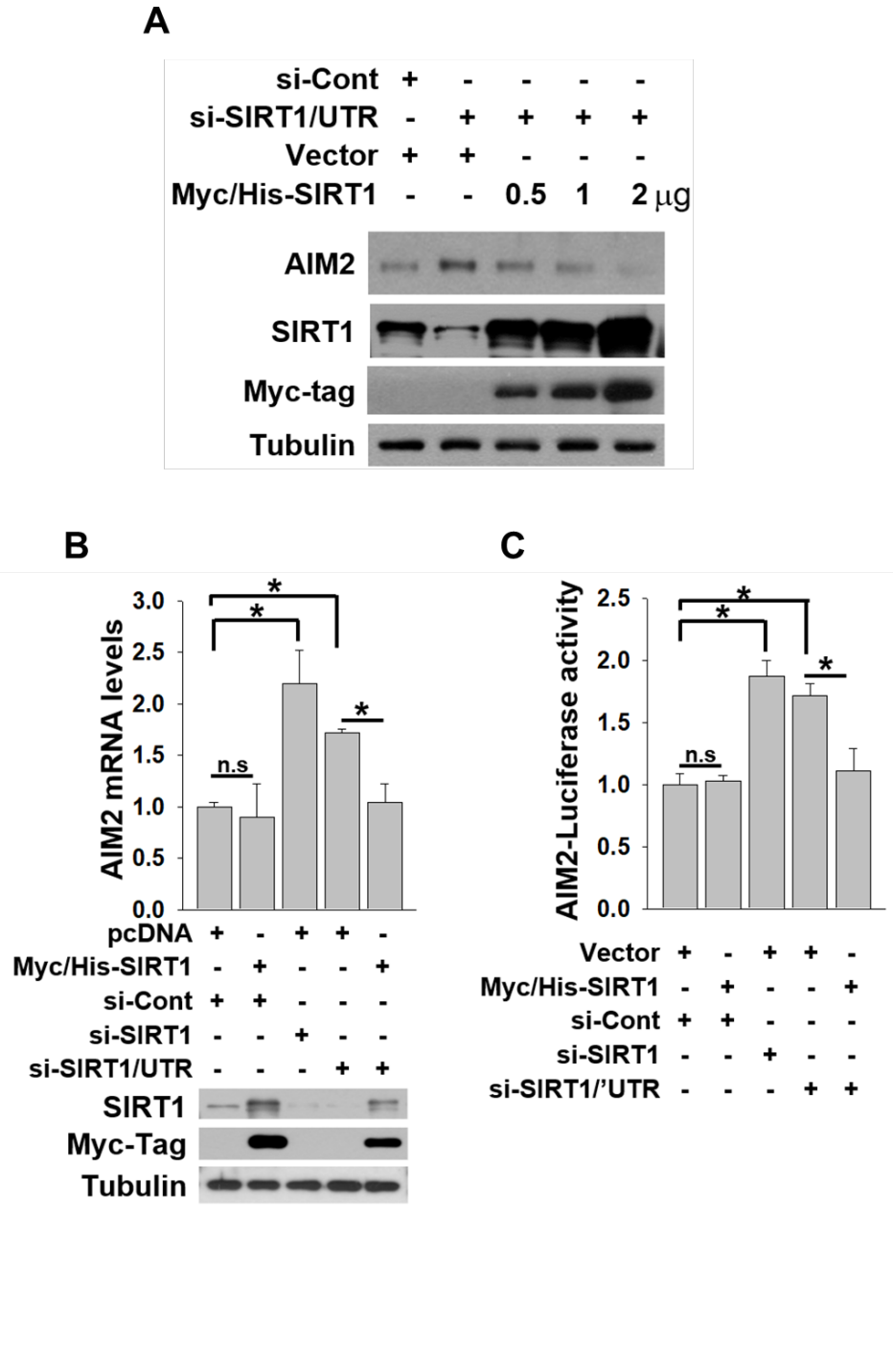
A
si-Cont + - - - -
si-SIRT1/UTR - + + + +
Vector + + - - -
Myc/His-SIRT1 - - 0.5 1 2 μg
AIM2
SIRT1
Myc-tag
Tubulin
B
AIM2 mRNA levels
3.0
2.5
2.0
1.5
1.0
0.5
0.0
n.s
*
pcDNA + - + + -
Myc/His-SIRT1 - + - - +
si-Cont + + - - -
si-SIRT1 - - + - -
si-SIRT1/UTR - - - + +
SIRT1
Myc-Tag
Tubulin
C
AIM2-Luciferase activity
2.5
2.0
1.5
1.0
0.5
0.0
n.s
*
Vector + - + + -
Myc/His-SIRT1 - + - - +
si-Cont + + - - -
si-SIRT1 - - + - -
si-SIRT1/'UTR - - - + +

Figure 19. SIRT1 represses the transcription of the *AIM2* gene.

(A) SiHa cells were co-transfected with the indicated siRNA and plasmid, further cultured for 48 hours, and subjected to Western blotting. (B) SiHa cells were transfected as indicated, incubated for 48 hours, and subjected to RT-qPCR. *P < 0.05 by Student's t test. (C) SiHa cells were co-transfected with the AIM2-Luc plasmid and others indicated, incubated for 48 hours, and subjected to luciferase analysis. *P < 0.05 by Student's t test.

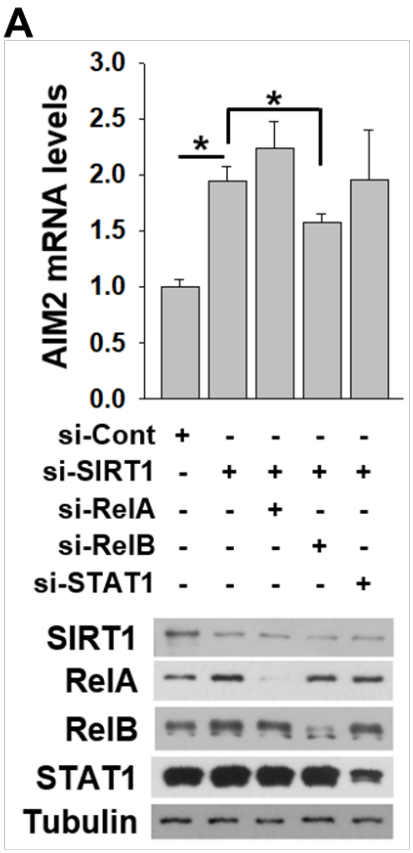
A
AIM2 mRNA levels
3.0
2.5
2.0
1.5
1.0
0.5
0.0
*
*
si-Cont + - - - -
si-SIRT1 - + + + +
si-RelA - - + - -
si-RelB - - - + -
si-STAT1 - - - - +
SIRT1
RelA
RelB
STAT1
Tubulin

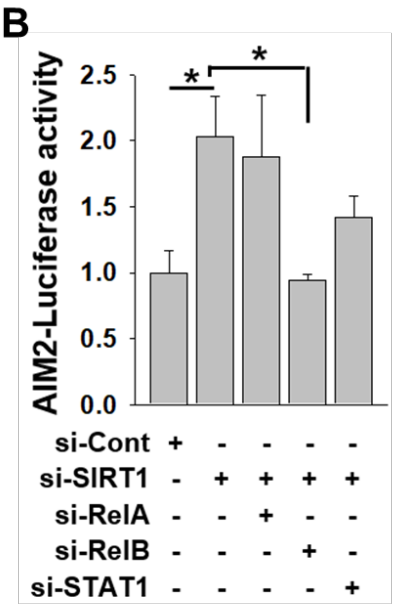
B
AIM2-Luciferase activity
2.5
2.0
1.5
1.0
0.5
0.0
*
*
si-Cont + - - - -
si-SIRT1 - + + + +
si-RelA - - + - -
si-RelB - - - + -
si-STAT1 - - - - +

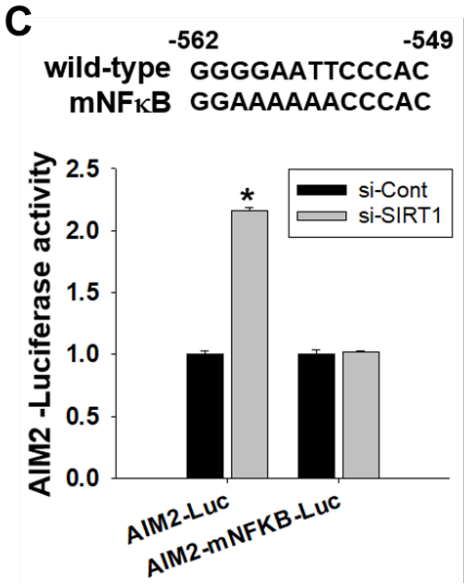
C
-562
-549
wild-type GGGGAATTCCCAC
mNFκB GGAAAAAACCCAC
AIM2 -Luciferase activity
2.5
2.0
1.5
1.0
0.5
0.0
*
si-Cont
si-SIRT1
AIM2-Luc
AIM2-mNFKB-Luc

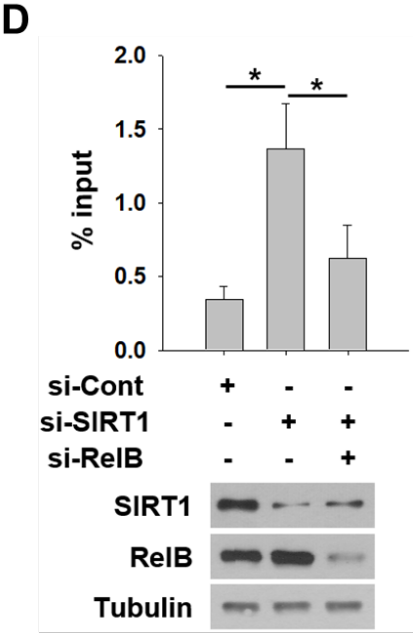
D
% input
2.0
1.5
1.0
0.5
0.0
*
*
si-Cont + - -
si-SIRT1 - + +
si-RelB - - +
SIRT1
RelB
Tubulin

**Figure 20. SIRT1 protects cervical cancer by suppressing the NF-κB- mediated AIM2 expression.**

(A) SiHa cells were transfected as indicated, incubated for 48 hours, and subjected to RT-qPCR. *P < 0.05 by Student's t test. (B) SiHa cells were co-transfected with the AIM2-Luc plasmid and others indicated, incubated for 48 hours, and subjected to luciferase analysis. *P < 0.05 by Student's t test. (C) The sequences of wild-type or mutated NFkB-binding site in the AIM2-Luc plasmids (top). SiHa cells co-transfected with 1μg of the AIM2-Luc plasmid and 40 nM siRNA, incubated for 48 hours, and subjected to luciferase analysis. Each symbol or bar represents the mean + SD (n=4). *P < 0.05 by Student's t test. (D) SiHa cells were transfected with the indicated siRNAs (40 nM each), and 48 hours later subjected to ChIP. *P < 0.05 by Student's t test.

A

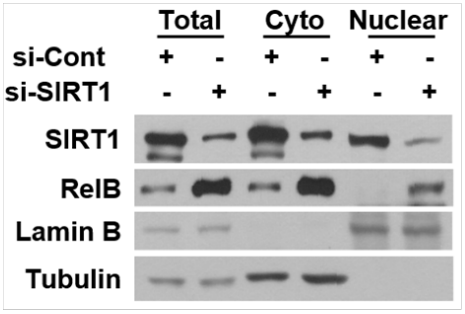
Total
Cyto
Nuclear
si-Cont + - + - + -
si-SIRT1 - + - + - +
SIRT1
RelB
Lamin B
Tubulin

B

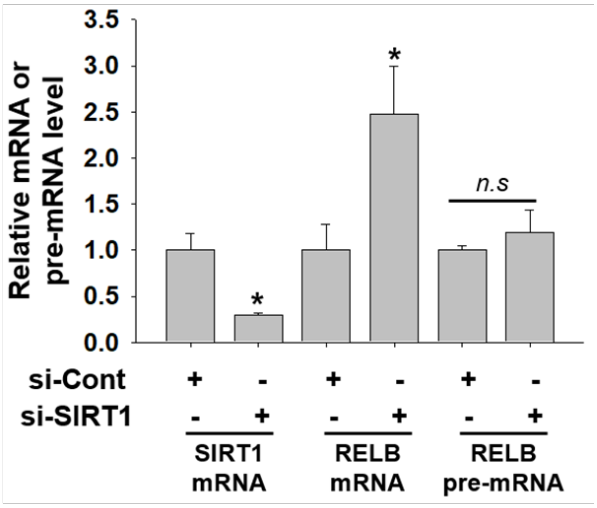
Relative mRNA or pre-mRNA level
3.5
3.0
2.5
2.0
1.5
1.0
0.5
0.0
*
*
n.s
si-Cont + - + - + -
si-SIRT1 - + - + - +
SIRT1 mRNA
RELB mRNA
RELB pre-mRNA

C

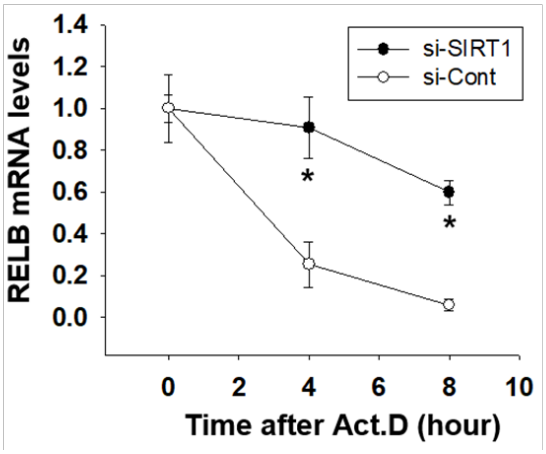
RELB mRNA levels
1.4
1.2
1.0
0.8
0.6
0.4
0.2
0.0
si-SIRT1
si-Cont
*
*
0
2
4
6
8
10
Time after Act.D (hour)

Figure 21. SIRT1 destabilizes the RELB mRNA.

(A) SiHa cells, which had been transfected with the siRNAs, were lysed and fractionated to cytoplasmic (Cyto) and nuclear (Nu) components. (B) SiHa cells, which had been transfected with the siRNAs, were subjected to RT-qPCR. *P < 0.05 by Student's t test. (C) Transfected SiHa cells were treated with actinomycin D (5 μg/mL), incubated for 4 or 8 hours, and subjected to RT-qPCR. * P < 0.05 (Student's t test) versus the si-Cont group.

A

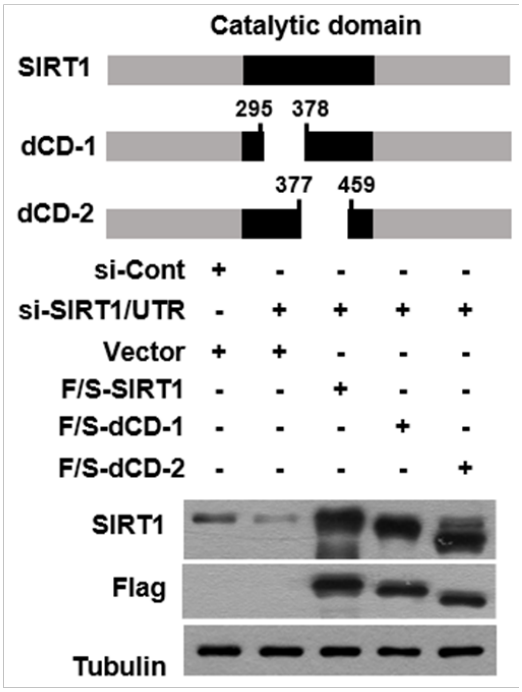
Catalytic domain
SIRT1
295
378
dCD-1
377
459
dCD-2
si-Cont + - - - -
si-SIRT1/UTR - + + + +
Vector + + - - -
F/S-SIRT1 - - + - -
F/S-dCD-1 - - - + -
F/S-dCD-2 - - - - +
SIRT1
Flag
Tubulin

B

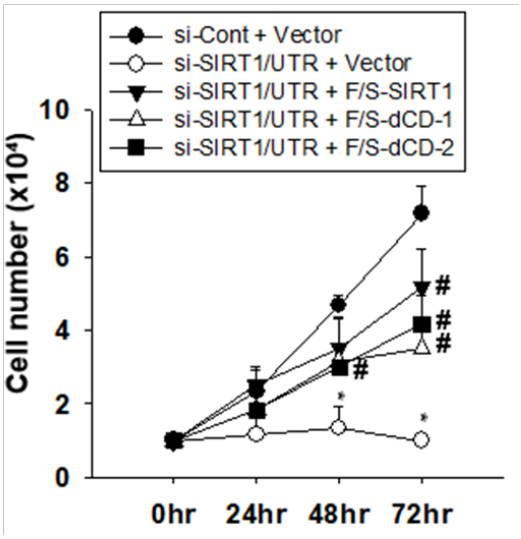
si-Cont + Vector
si-SIRT1/UTR + Vector
si-SIRT1/UTR + F/S-SIRT1
si-SIRT1/UTR + F/S-dCD-1
si-SIRT1/UTR + F/S-dCD-2
Cell number (x10⁴)
10
8
6
4
2
0
0hr
24hr
48hr
72hr
#
*

**Figure 22. SIRT1 promotes cervical cancer cell survival in a deacetylase-independent manner.**

(A) F/S-tagged SIRT1 constructs are presented (top). SiHa cells were co-transfected with an siRNA targeting the 5' UTR of *SIRT1* mRNA and the SIRT1 plasmids (1 μg per 100-mm dish). SIRT1 knock-down and SIRT1 overexpression were checked by immunoblotting (bottom). (B) SiHa cells, which had been co-transfected with the indicated siRNA and plasmid, were cultured for 1-3 days, and counted. Each point represents the mean + SD (n=4). *, $P < 0.05$ versus the si-Cont/Vector group; #, $P < 0.05$ versus the si-SIRT1_5' UTR/Vector group. *, # $P < 0.05$ by Student's t test.

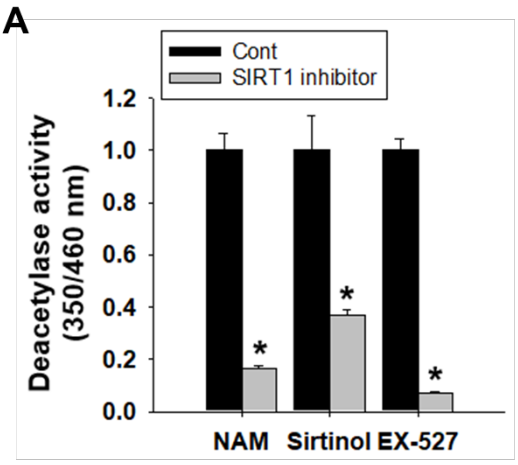
A
Cont
SIRT1 inhibitor
Deacetylase activity
(350/460 nm)
1.2
1.0
0.8
0.6
0.4
0.2
0.0
*
*
*
NAM
Sirtinol
EX-527

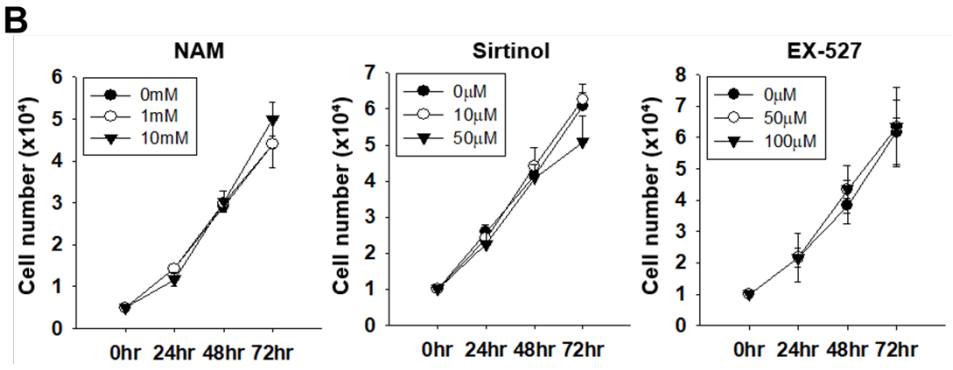
B
NAM
Cell number (x10⁴)
0mM
1mM
10mM
0hr 24hr 48hr 72hr
Sirtinol
Cell number (x10⁴)
0μM
10μM
50μM
0hr 24hr 48hr 72hr
EX-527
Cell number (x10⁴)
0μM
50μM
100μM
0hr 24hr 48hr 72hr

**Figure 23. Effects of SIRT1 deacetylase inhibitors on cancer cell growth.**

(A) SiHa cells were treated with nicotinamide (10 mM), sirtinol (50 μM), or EX-527 (100 μM) for 48 hours. Bars represent the means ± SD from 4 separate experiments. *P < 0.05, Mann-Whitney U test. (B) SiHa cells were seeded at $1\times10^4$ cells/well in 24-well plates, and treated with Nicotinamide, Sirtinol, or EX-527 at the indicated concentrations for 1-3 days. Each point represents the mean ± SD of cell number (n=4).

A

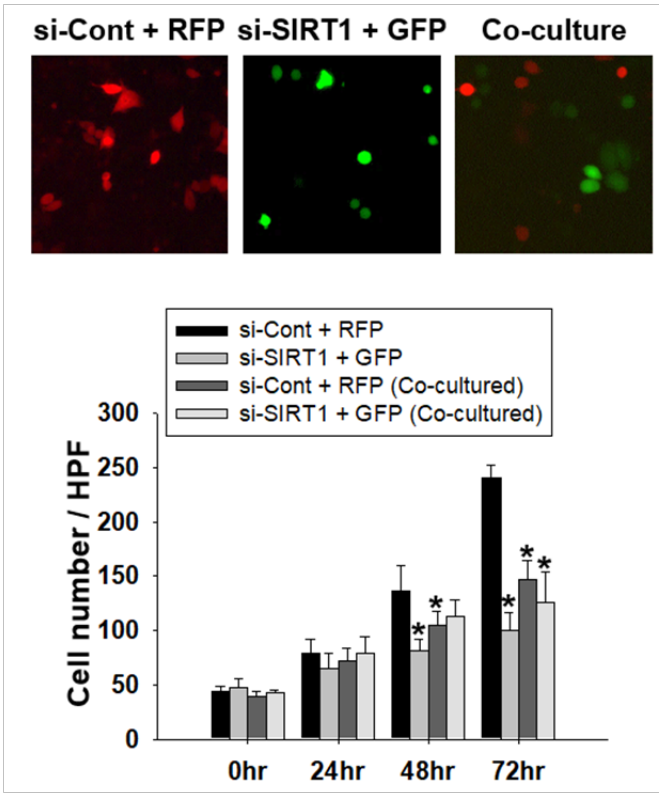
si-Cont + RFP
si-SIRT1 + GFP
Co-culture
si-Cont + RFP
si-SIRT1 + GFP
si-Cont + RFP (Co-cultured)
si-SIRT1 + GFP (Co-cultured)
Cell number / HPF
300
250
200
150
100
50
0
0hr
24hr
48hr
72hr

B

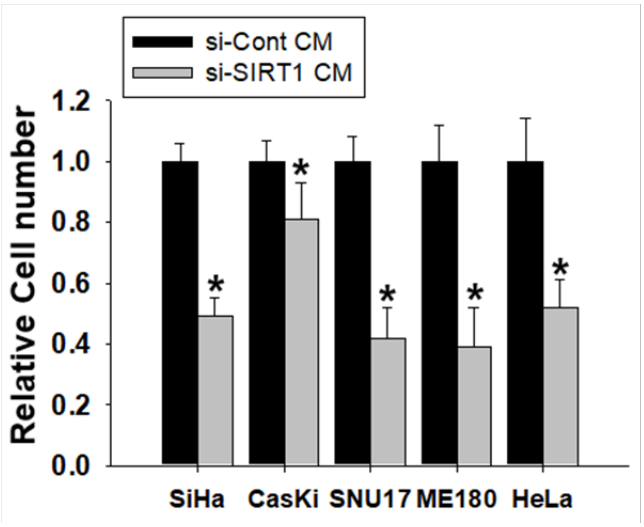
si-Cont CM
si-SIRT1 CM
Relative Cell number
1.2
1.0
0.8
0.6
0.4
0.2
0.0
SiHa
CasKi
SNU17
ME180
HeLa

**Figure 24. SIRT1 knockdown-derived conditioned media inhibit cervical cancer cell growth.**

(A) SiHa cells were co-transfected with the non-targeting siRNA (40 nM) and the RFP plasmid (1 μg) or with the SIRT1-targeting siRNA and the GFP plasmid. After stabilized for 12 hours, the transfected cells were co-cultured (1:1) for 1-3 days. The representative fluorescence images of 3 day-culture were presented (left). Based on the fluorescence images, the numbers of GFP- and RFP-labeled cells were counted on day 1-3 (right). *P < 0.05 by Student's t test. (B) Cervical cancer cells were seeded at $1\times10^4$ cells/well in 24-well plate, and treated with the conditioned media from SIRT1 knocked-down SiHa cells. After incubated for 48 hours, cells were counted. *P < 0.05 by Student's t test.

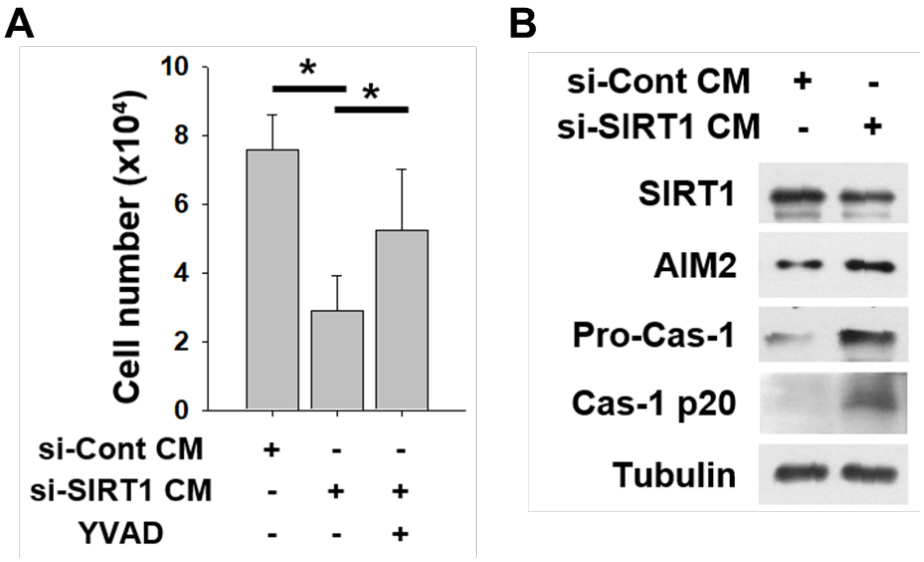


Figure 25. Intercellular transmission of pyroptosis under SIRT1 knockdown.

(A) SiHa cells were incubated in the conditioned media (CM) with/without Ac-YVAD-cmk (10 μg/mL) for 72 hours, and counted. *P < 0.05 by Student's t test. (B) SiHa cells were incubated in the conditioned media for 48 hours, and subjected to Western blotting.

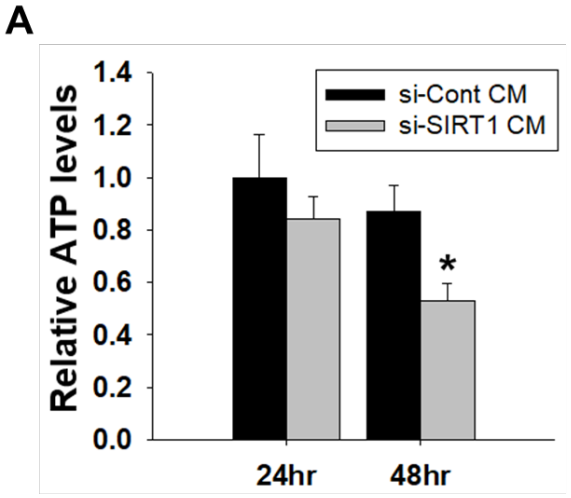
A
Relative ATP levels
1.4
1.2
1.0
0.8
0.6
0.4
0.2
0.0
si-Cont CM
si-SIRT1 CM
*
24hr
48hr

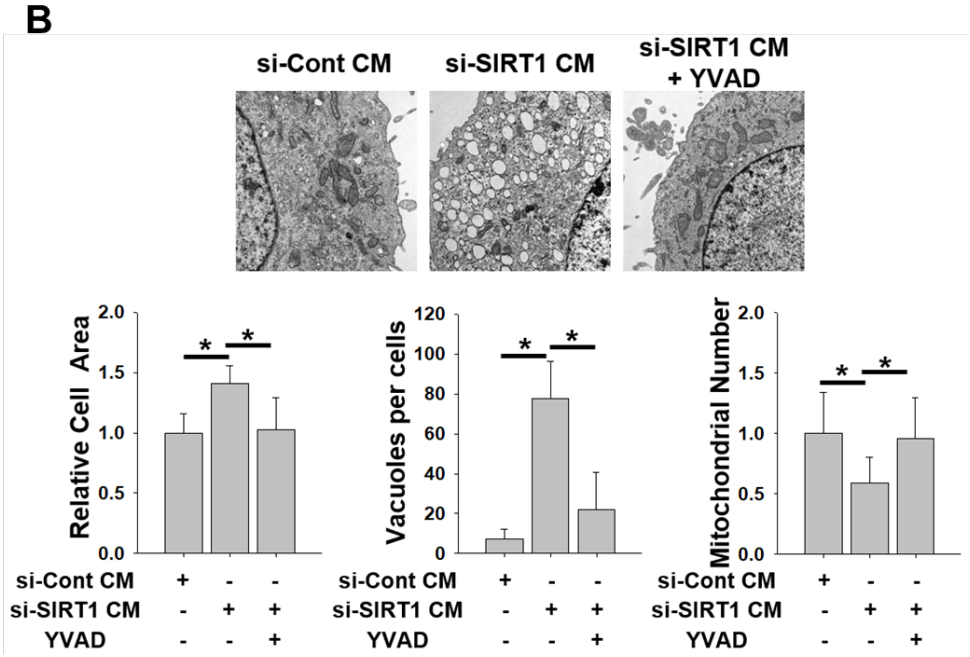
B
si-Cont CM
si-SIRT1 CM
si-SIRT1 CM
+ YVAD
Relative Cell Area
Vacuoles per cells
Mitochondrial Number
si-Cont CM
si-SIRT1 CM
YVAD

**Figure 26. SIRT1 knockdown-derived conditioned media trigger pyroptotic events.**

(A) SiHa cells were incubated in the conditioned media for 24 or 48 hours, and lysed to measure the intracellular ATP level. *P < 0.05 by Mann-Whitney U test. (B) SiHa cells were incubated in the conditioned media with/without Ac-YVAD-cmk (10 μg/mL) for 48 hours, and subjected to transmission electron microscopy. Cross sectional area of cells, vacuole number per cells, and mitochondrial number per cells were measured using ImageJ. Each bar represents the mean + SD (n =12). *P < 0.05 by.

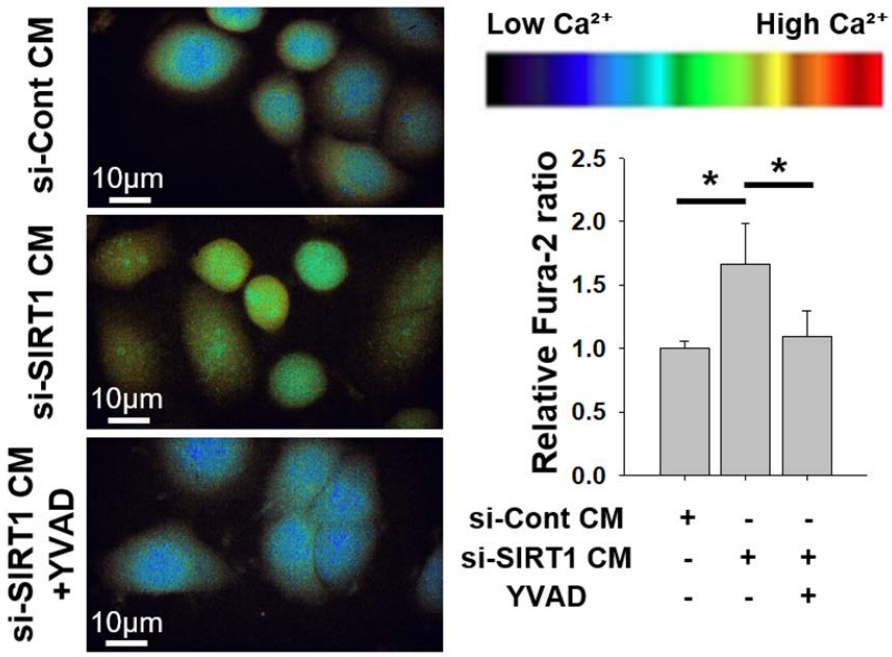


Figure 27. SIRT1 knockdown-derived conditioned media causes an imbalance of the ionic homeostasis.

SiHa cells, which had been plated at $5\times10^5$ cells per 35-mm dish, were incubated in the conditioned media with/without Ac-YVAD-cmk for 48 hours. Cells were incubated with Fura-2 and photographed under a fluorescence microscope (left). The ratio of fluorescence intensities at the excitation wavelengths 340 and 380 nm was measured to quantify intracellular calcium levels (right). Each bar represents the mean + SD from 20 independent experiments. *, $P < 0.05$ (by Mann-Whitney U test) versus the si-Cont group; #, $P < 0.05$ versus the si-SIRT1 group.

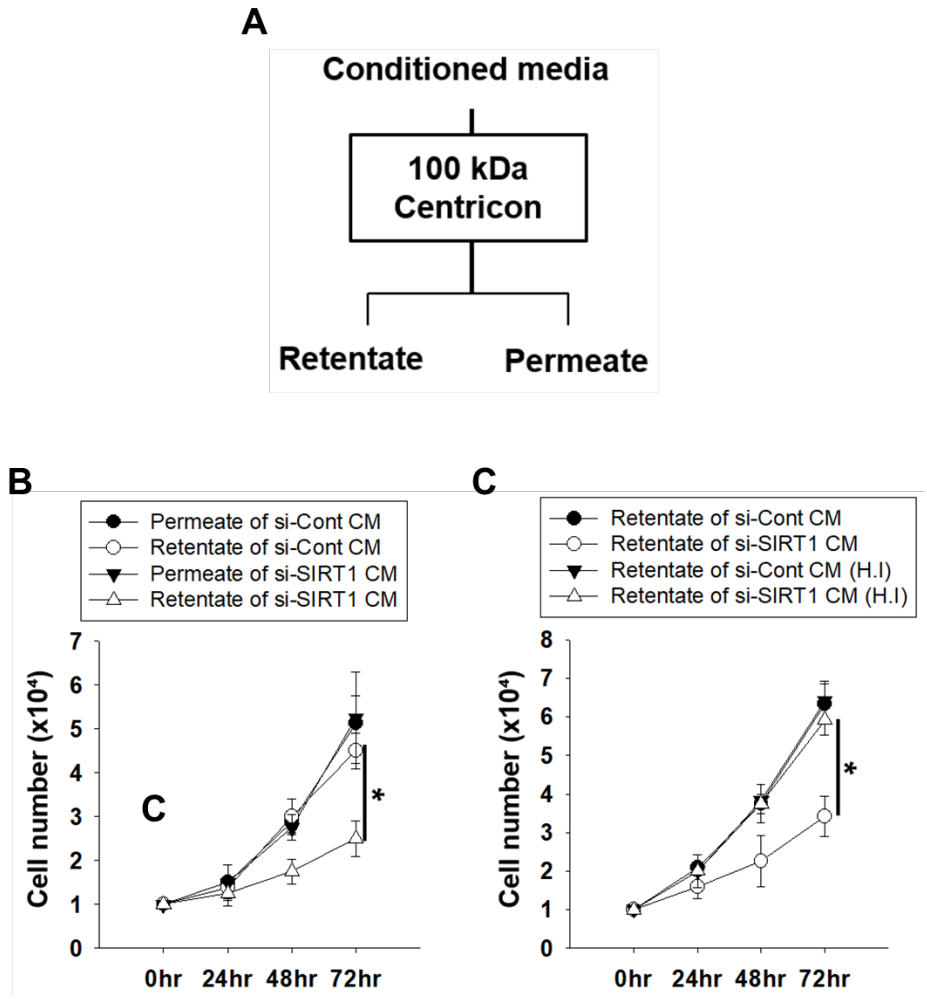
A
Conditioned media
100 kDa
Centricon
Retentate
Permeate
B
Permeate of si-Cont CM
Retentate of si-Cont CM
Permeate of si-SIRT1 CM
Retentate of si-SIRT1 CM
Cell number (x10⁴)
C
*
0hr 24hr 48hr 72hr
C
Retentate of si-Cont CM
Retentate of si-SIRT1 CM
Retentate of si-Cont CM (H.I)
Retentate of si-SIRT1 CM (H.I)
Cell number (x10⁴)
*
0hr 24hr 48hr 72hr

**Figure 28. Identifying the pyroptosis-transmitting factor in SIRT1 knockdown-derived condition media.**

(A) Schematic diagram for fractionation of high molecular weight components in the conditioned medium from SIRT1 knocked-down SiHa cells. (B) SiHa cells were treated with 100 kDa cut-off permeate or retentate of conditioned medium from SIRT1 knockdown cells, and counted. Each point represents the mean ± SD (n=4). *P < 0.05 by Student's t test. (C) SiHa cells were treated with retentate or heat-inactivated (H.I.) reatentate, and counted after the indicated times. *P < 0.05 by Student's t test.

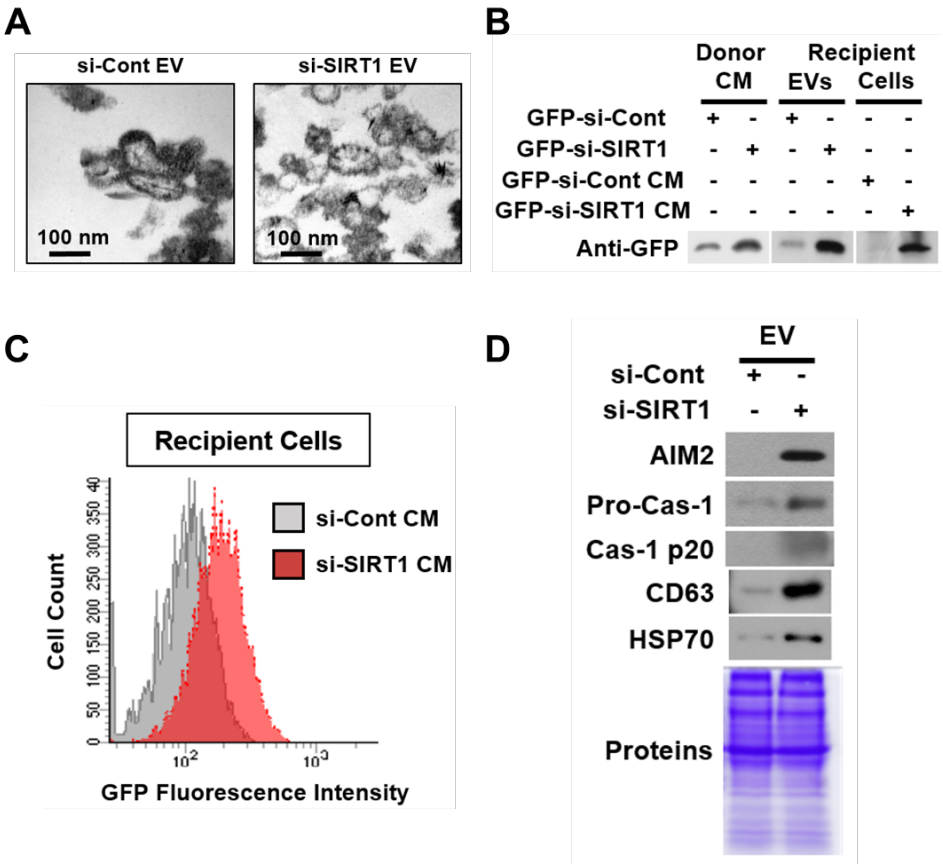
A
si-Cont EV
si-SIRT1 EV
100 nm
100 nm
B
Donor CM
Recipient EVs
Recipient Cells
GFP-si-Cont + - + - - -
GFP-si-SIRT1 - + - + - -
GFP-si-Cont CM - - - - + -
GFP-si-SIRT1 CM - - - - - +
Anti-GFP
C
Recipient Cells
si-Cont CM
si-SIRT1 CM
Cell Count
0 50 100 150 200 250 300 350 400
10^2
10^3
GFP Fluorescence Intensity
D
EV
si-Cont + -
si-SIRT1 - +
AIM2
Pro-Cas-1
Cas-1 p20
CD63
HSP70
Proteins

**Figure 29. Inflammasomal components are transmitted through extracellular vesicles.**

(A) Transmission electron microscopy images of extracelluar vesicles in the conditioned media from SiHa cells. (B) GFP-expressing SiHa cells were transfected with 40 nM siRNA. After remaining siRNAs were removed by changing media, cells were further cultured for 24 hours. Western blotting was performed in the conditioned media (CM), purified extracellular vesicles, or lysates of recipient SiHa cells that were incubated in the CM for 48 hours. (C) Naïve SiHa cells were incubated in the conditioned media from GFP-expressing SiHa cells for 48 hours, and subjected to flow cytometry analysis for detection of transferred GFP. (D) Western blot analysis and Coomassie blue staining in the extracellular vesicles isolated from the conditioned media from SiHa cells. Vesicle lysates (15 μg of proteins per lane) was electrophoresed under denaturing conditions.

A

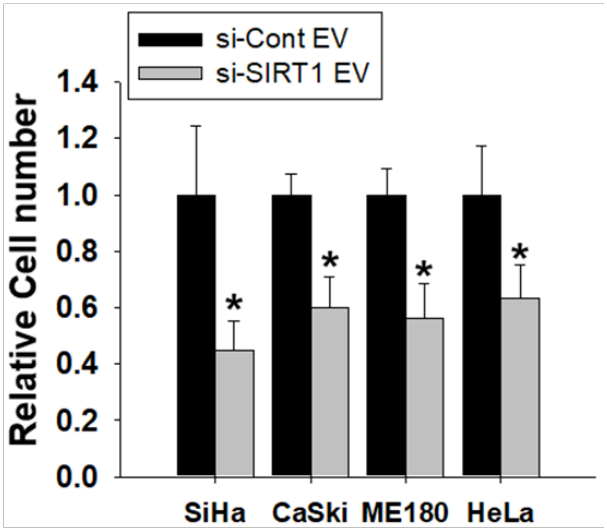
si-Cont EV
si-SIRT1 EV
Relative Cell number
1.4
1.2
1.0
0.8
0.6
0.4
0.2
0.0
*
SiHa
CaSki
ME180
HeLa

B

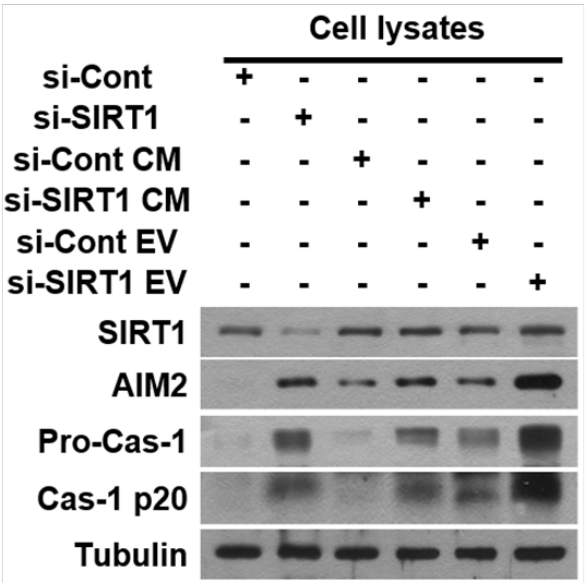
Cell lysates
si-Cont + - - - - -
si-SIRT1 - + - - - -
si-Cont CM - - + - - -
si-SIRT1 CM - - - + - -
si-Cont EV - - - - + -
si-SIRT1 EV - - - - - +
SIRT1
AIM2
Pro-Cas-1
Cas-1 p20
Tubulin

**Figure 30. Inflammasome-mediated pyroptosis is propagated via extracellular vesicles.**

(A) Naïve SiHa cells were treated with extracellular vesicles (20 μg) isolated from SIRT1 knocked-down SiHa cells, and incubated for 72 hours. Each bar represents the mean ± SD (n=4). *P < 0.05 versus the si-Con EV group (Student's t test). (B) Western blot analyses of AIM2 inflammasome-related proteins. Lanes 1-2: SiHa cells were transfected with 40 nM siRNA and incubated for 48 hours. Lanes 3-4: SiHa cells were treated with conditioned media from SIRT1 knocked-down cells and incubated for 48 hours. Lanes 5-6: SiHa cells were treated with extracellular vesicles isolated from SIRT1 knocked-down cells and incubated for 48 hours.

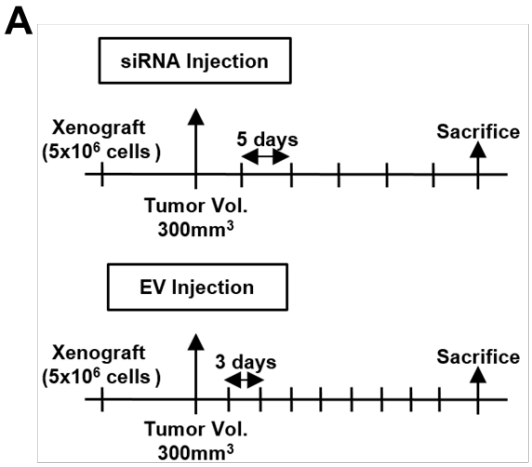
A
siRNA Injection
Xenograft
(5x10^6 cells)
5 days
Sacrifice
Tumor Vol.
300mm^3
EV Injection
Xenograft
(5x10^6 cells)
3 days
Sacrifice
Tumor Vol.
300mm^3

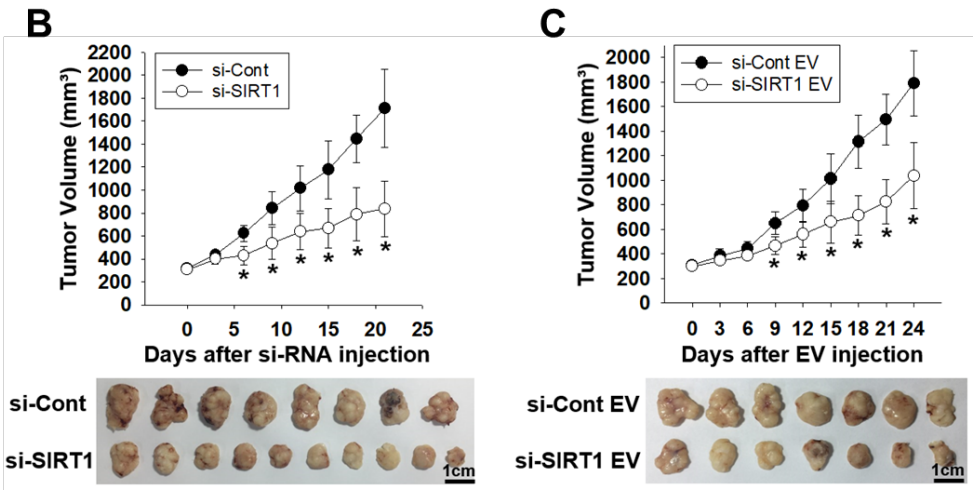
B
Tumor Volume (mm³)
si-Cont
si-SIRT1
Days after si-RNA injection
si-Cont
si-SIRT1
1cm
C
Tumor Volume (mm³)
si-Cont EV
si-SIRT1 EV
Days after EV injection
si-Cont EV
si-SIRT1 EV
1cm

**Figure 31. Anticancer effects of SIRT1-targeting siRNA and SIRT1 knockdown-derived extracellular vesicles.**

(A) Schemes for the in vivo experimental procedures to evaluate anticancer activities of SIRT1-targeting siRNA and SIRT1-knockdown-derived extracellular vesicles. (B) SiHa cells ($5\times10^6$ cells per mouse) were subcutaneously inoculated in the flank of mouse. When tumor volume attains at 300 $mm^3$, the siRNA (10 μg per tumor) was injected into tumors once every 5 days. Each point represents the mean ± SD (si-Cont mouse, n=8; si-SIRT1 mouse, n=10). *P < 0.05 by Mann-Whitney U test. Tumors were excised from mice and photographed (bottom). (C) The extracellular vesicles (15 μg per tumor) were injected into tumors once every 3 days. Each point represents the mean ± SD (n=7 per group). *P < 0.05 by Mann-Whitney U test. Tumors were excised from mice and photographed (bottom).

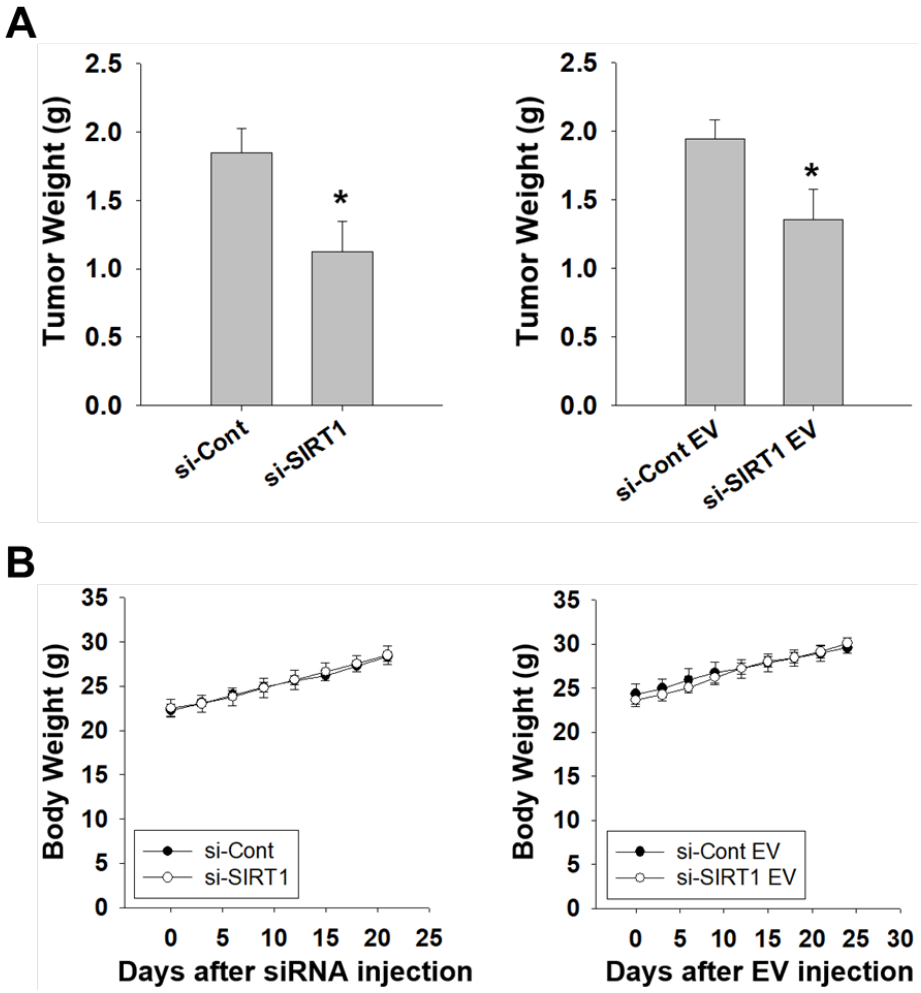
A
Tumor Weight (g)
2.5
2.0
1.5
1.0
0.5
0.0
*
si-Cont
si-SIRT1
Tumor Weight (g)
2.5
2.0
1.5
1.0
0.5
0.0
*
si-Cont EV
si-SIRT1 EV
B
Body Weight (g)
35
30
25
20
15
10
5
0
si-Cont
si-SIRT1
0 5 10 15 20 25
Days after siRNA injection
Body Weight (g)
35
30
25
20
15
10
5
0
si-Cont EV
si-SIRT1 EV
0 5 10 15 20 25 30
Days after EV injection

Figure 32. Parameters in xenografted SiHa tumors.

(A) Tumors were removed from mice and weighed. Each bar represents the mean + SD (si-Cont, n=8; si-SIRT1, n=10, si-Cont EV, n=7; si-SIRT1 EV, n=7). *P < 0.05 (Mann-Whitney U test) versus the si-Cont or si-Cont EV group. (B) Time courses of body weights in tumor-bearing mice. Each point represents the mean ± SD (si-Cont, n=8; si-SIRT1, n=10; si-Cont EV, n=7; si-SIRT1 EV, n=7).

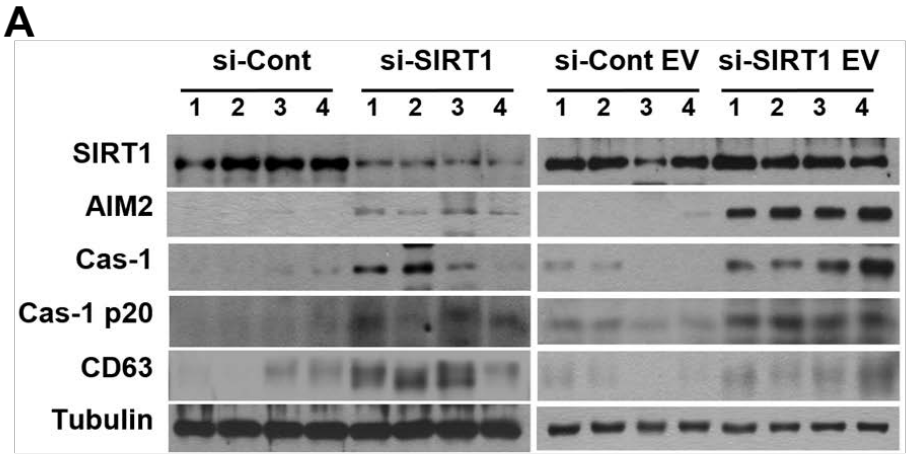
A
si-Cont
si-SIRT1
si-Cont EV
si-SIRT1 EV
1 2 3 4 1 2 3 4 1 2 3 4 1 2 3 4
SIRT1
AIM2
Cas-1
Cas-1 p20
CD63
Tubulin

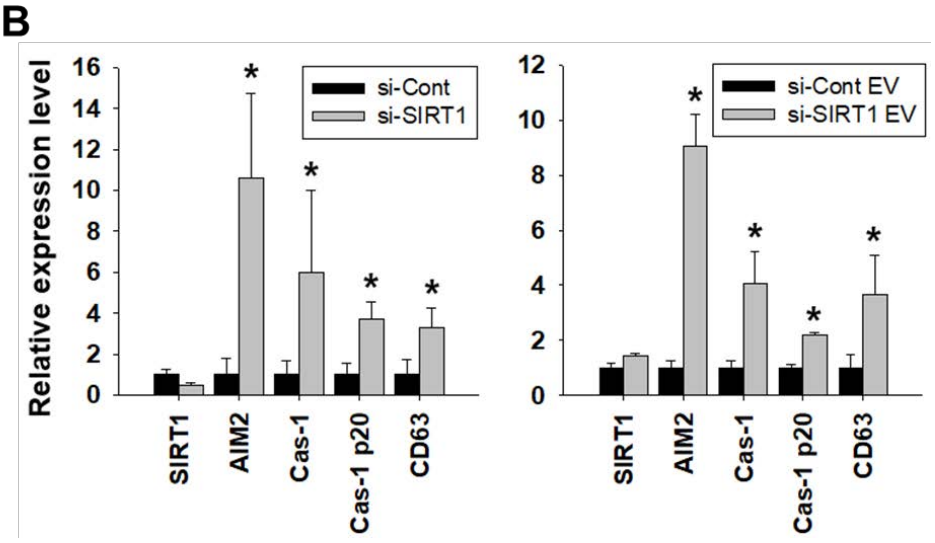
B
Relative expression level
si-Cont
si-SIRT1
si-Cont EV
si-SIRT1 EV
SIRT1
AIM2
Cas-1
Cas-1 p20
CD63

Figure 33. Activation of AIM2 inflammasome in xenografted tumors.

(A) Western blot analyses of AIM2 inflammasome-related proteins in xenografted tumors. The error bars represent the means ± SD (n=4 per group). (B) Western blot analyses of AIM2 inflammasome-related proteins in xenografted tumors. Proteins were quantified using ImageJ. Each bar represents the mean ± SD (n=4 per each group). *P < 0.05 by Mann-Whitney U test.

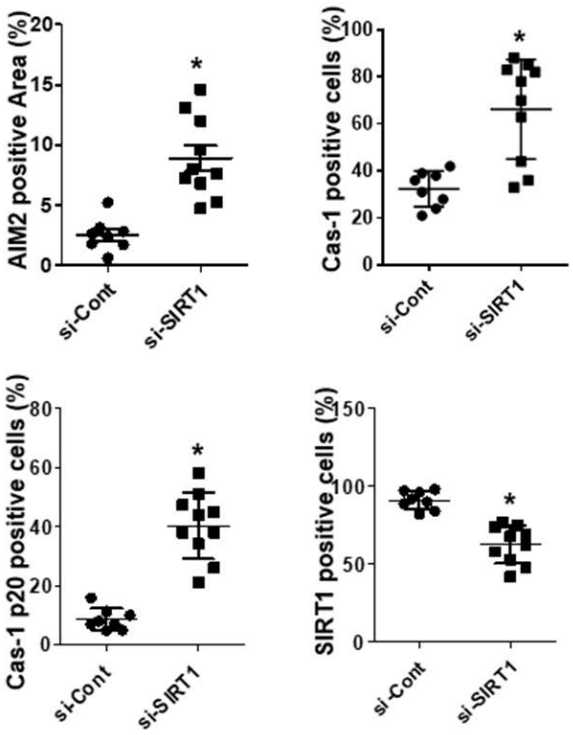
AIM2 positive Area (%)
Cas-1 positive cells (%)
Cas-1 p20 positive cells (%)
SIRT1 positive cells (%)
si-Cont
si-SIRT1
*

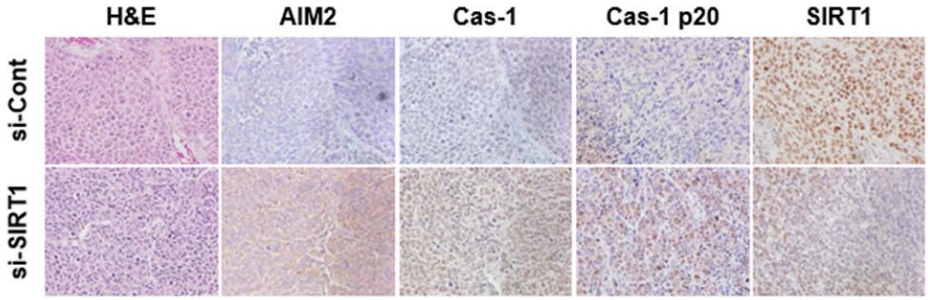
H&E
AIM2
Cas-1
Cas-1 p20
SIRT1
si-Cont
si-SIRT1

**Figure 34. Immunohistochemical analyses of AIM2 inflammasome-related proteins in siRNA injected tumors.**

si-Cont, n=8; si-SIRT1, n=10. Horizontal bars represent the means and SD and * denotes P < 0.05. *P < 0.05 by Mann-Whitney U test. The bottom panels represent images of immunohistochemical staining in xenografted tumors (Scale bar = 50 μm).

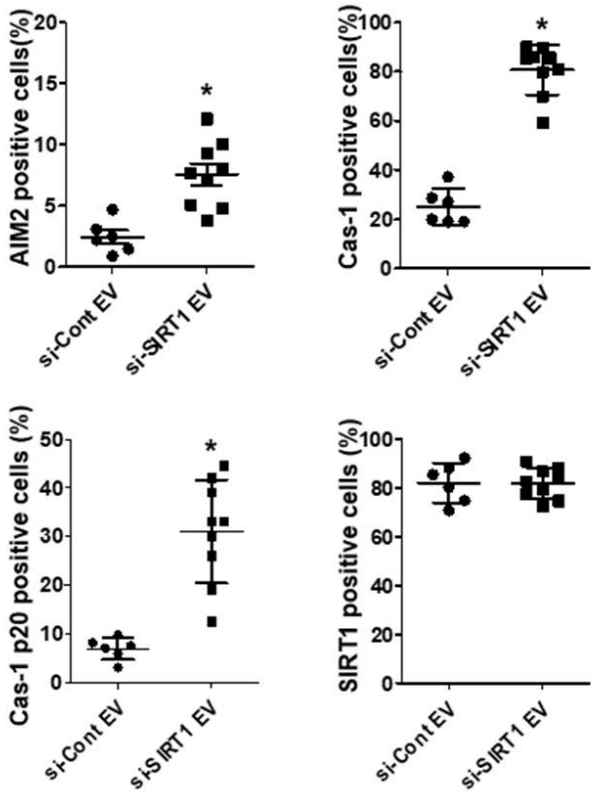
AIM2 positive cells(%)
Cas-1 positive cells(%)
Cas-1 p20 positive cells (%)
SIRT1 positive cells (%)
si-Cont EV
si-SIRT1 EV
*

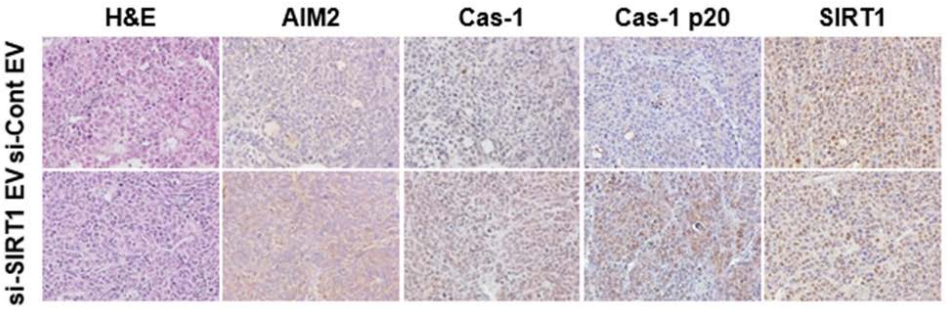
H&E
AIM2
Cas-1
Cas-1 p20
SIRT1
si-Cont EV
si-SIRT1 EV

**Figure 35. Immunohistochemical analyses of AIM2 inflammasome-related proteins in SIRT1 knockdown-derived extracellular vesicles injected tumors.**

si-Cont EV, n=6; si-SIRT1 EV, n=7. Horizontal bars represent the means and SD and * denotes $P < 0.05$. *$P < 0.05$ by Mann-Whitney U test. The bottom panels represent images of images of immunohistochemical staining in xenografted tumors (Scale bar = 50 μm).

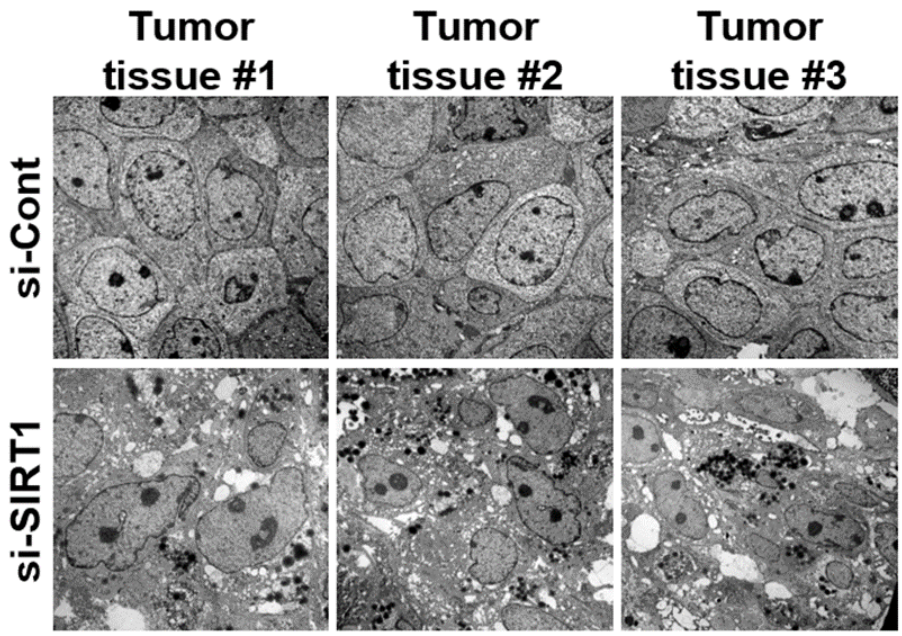


Figure 36. Transmission electron microscopy images of tumors injected with siRNAs.

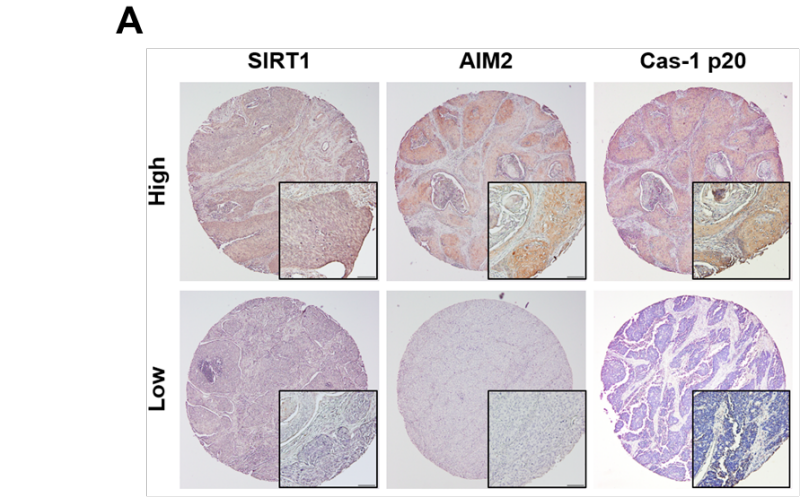
A
SIRT1
AIM2
Cas-1 p20
High
Low

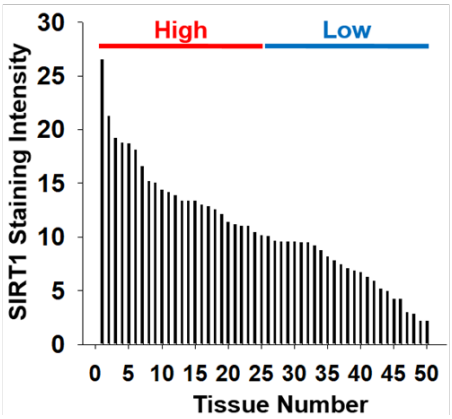
B
High
Low
SIRT1 Staining Intensity
30
25
20
15
10
5
0
0 5 10 15 20 25 30 35 40 45 50
Tissue Number

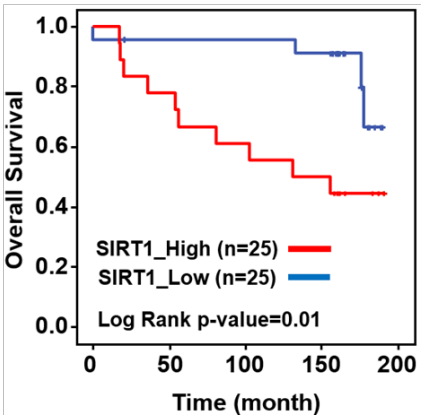
C
Overall Survival
1.0
0.8
0.6
0.4
0.2
0.0
SIRT1_High (n=25)
SIRT1_Low (n=25)
Log Rank p-value=0.01
0
50
100
150
200
Time (month)

**Figure 37. High expression of SIRT1 is associated with poor survival in cervical cancer patients.**

(A) Representative photographs of immunohistochemical staining in cervical cancer tissue arrays. (B) Distribution of SIRT1 expression in 50 cervical cancer tissues. SIRT1 high and low groups were divided based on the median value. (C) Kaplan–Meier analysis of the overall survival of patients with cervical cancer was performed in SIRT1 high and low groups. The P value was calculated by Log Rank test.

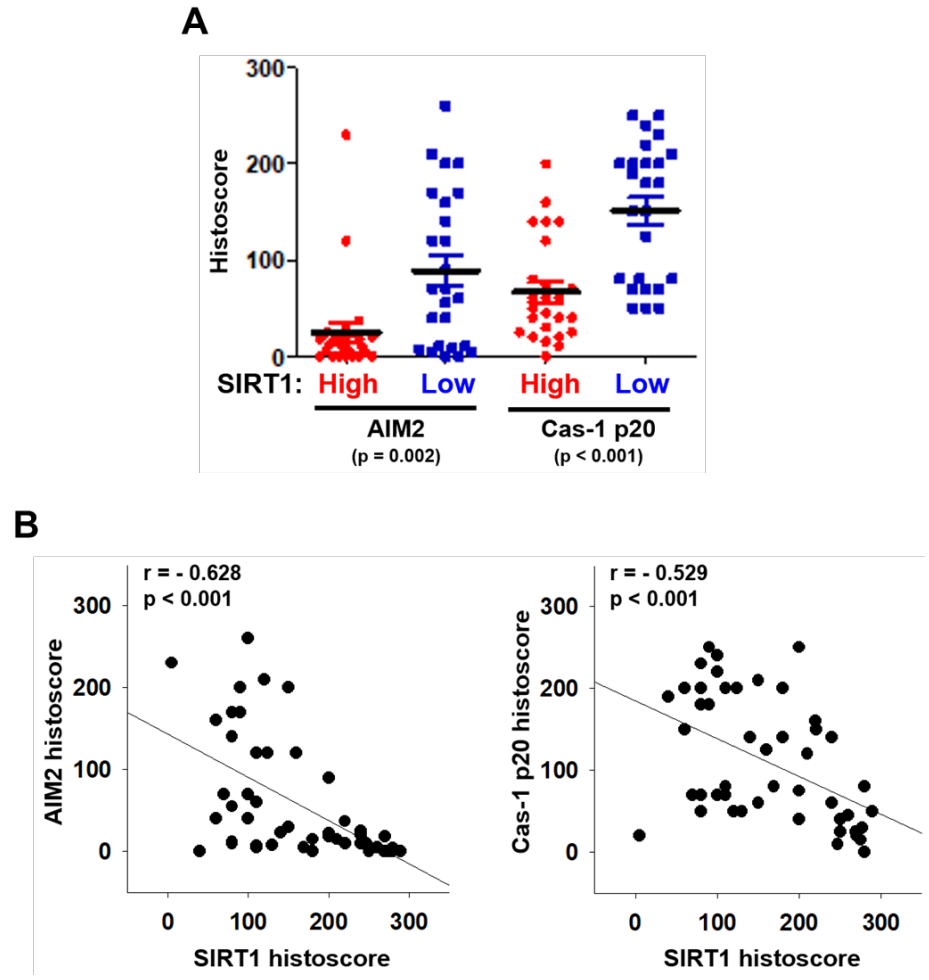


Figure 38. Negative correlation between SIRT1 and AIM2 in patient tissue of cervical cancer.

(A) Based on the histoscores, AIM2 and Caspase-1 p20 levels were compared between SIRT1 high and low groups. The P value was calculated by Mann-Whitney U test. (B) Spearman's correlation analyses between SIRT1 and AIM2 or SIRT1 and Caspase-1 p20 levels. 'r' and 'p' mean coefficient and p-value, respectively.

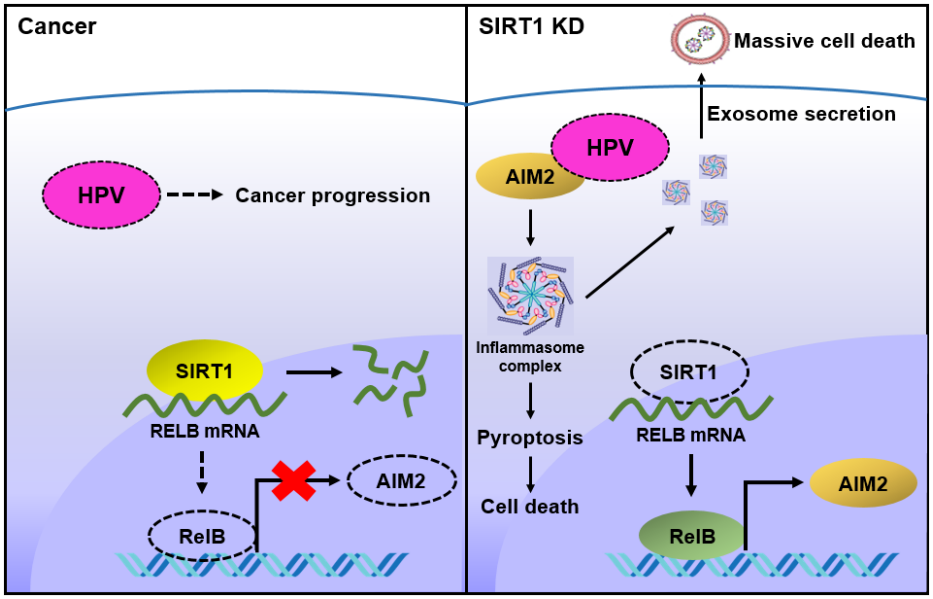


Figure 39. Graphical summary of SIRT1 knockdown effect on cervical cancer.

# DISCUSSION

In this study, I addressed the question regarding why cervical cancer cells require a higher level of SIRT1 for survival. SIRT1 repressed the transcription of the *AIM2* gene, thereby helping HPV-infected cancer cells evade the antiviral immune response. Unexpectedly, the AIM2 inflammasome-mediated pyroptosis was intercellularly propagated through extracellular vesicles. I found an inverse correlation between SIRT1 and AIM2 expression in human cervical cancer tissues and the association of SIRT1 with the poor prognosis of patients. In a xenograft mouse model, I tested the possibility of a new cervical cancer therapy using SIRT1-targeting siRNA or extracellular vesicles harboring the inflammasome complex. Taken together, because SIRT1 functions to nullify antiviral immunity in HPV-infected cervical cancer cells, SIRT1-overexpressing cells seem to be selected and finally make highly malignant cancer clones.

It was previously suggested that SIRT1 inhibits apoptosis through its deacetylation of TP53, promoting cell survival in cervical cancer.[26] In this study, apoptosis occurred only in two of four squamous cell carcinoma cell lines under SIRT1

knockdown, and the population of apoptotic cells was less than 2% of total cells. In addition, the cytotoxic effect of SIRT1 knockdown was not observed in other cancer cell lines expressing TP53. Therefore, TP53 deacetylation seems not to be the major pathway of SIRT1-induced survival that occurs only in cervical cancer cells. By contrast, because AIM2 inflammasome-mediated cell death is a unique event occurring in virus-infected cells like cervical cancer cells, our scenario concerning the role of SIRT1 in cervical cancer survival seems to be reasonable.

AIM2 expression was enhanced by SIRT1 knockdown, and this effect was reversed by the reintroduction of SIRT1. However, in naïve cervical cancer cells, ectopic expression of SIRT1 did not reduce the basal level of AIM2. It is speculated that SIRT1 is upregulated in HPV-infected cells to the level sufficient for repressing AIM2. Our next concern was the mechanism by which SIRT1 negatively regulates AIM2. Our data suggest that SIRT1 negatively controls the *AIM2* gene transcription by destabilizing the mRNA of RelB - the transcription factor for the *AIM2* gene. Also, such actions of SIRT1 on AIM2 does not require the deacetylase activity of

SIRT1. Actually, the deacetylase-independent function of SIRT1 is not surprising because similar findings have been reported in several literature sources.[27-29] SIRT1 seems to have an alternate function using its non-catalytic domains that physically interact with target proteins.

AIM2 acts as a cytoplasmic sensor to recognize foreign double-stranded DNAs like HPV.[30] When viruses or bacteria invade cells, AIM2 starts to assemble the inflammasome complex consisting of caspase-1, PYCARD, and NLRP family, thereby activating caspase-1 to process proinflammatory cytokines and induce pyroptosis.[31,32] Beyond the first-line immunity against microorganisms, AIM2 has been reported to express tumor-suppressive activity in colon, liver and breast cancers irrespective of inflammasome.[33-35] However, it remains unclear whether AIM2 restricts tumor growth or metastasis through inflammasome. At least in HPV-infected cervical cancer cells, AIM2 may play a tumor-suppressive role by stimulating inflammasome-mediated pyroptosis. Such a role of AIM2 was also supported by a previous report showing that HPV16 activated the AIM2 inflammasome in keratinocytes.[36] The continuous suppression of AIM2 in keratinocytes might be

an essential prerequisite for tumor initiation and progression, so the derepression of the AIM2 gene could halt HPV-mediated cancer progression.

Extracellular vesicles, such as exosomes and microvesicles, contain diverse biological substances, and act as important mediators of cell-to-cell communication.[37-39] Recently, NLRP1 inflammasome proteins were detected in exosomes derived from the cerebrospinal fluid of patients with spinal cord or brain injury.[40] This report suggested that the inflammasome proteins can be released with extracellular vesicles. However, the role of inflammasome-containing extracellular vesicles has not been investigated thus far. To our best knowledge, this is the first report about extracellular vesicle-mediated propagation of inflammasome-induced death.

Invasive squamous carcinoma in uterine cervix is usually treated with a combination of chemotherapy, surgery, and/or radiation therapy.[41,42] Because effective target therapy has not been developed, the chemotherapy is still dependent on conventional cancer drugs.[43-45] Despite many efforts to understand tumor biology, the Achilles' heel of cervical cancer has not been identified. In this context, I propose that

SIRT1 could be a promising target for targeted therapy of cervical cancer. If viral therapy for silencing SIRT1 becomes clinically available, I could realize SIRT1-targeted therapy.

In conclusion, I found that SIRT1 is overexpressed in HPV-infected cervical cancer cells, enabling the cells to continue growing by nullifying AIM2 inflammasome-mediated immunity. Without SIRT1, cervical cancer cells can no longer survive because of the derepression of the AIM2 inflammasome. SIRT1 could be a remarkable target for cervical cancer therapy.

# REFERENCES


1. Small W Jr, Bacon MA, Bajaj A, Chuang LT, Fisher BJ, Harkenrider MM *et al*. Cervical cancer: A global health crisis. *Cancer* 2017; 123: 2404-2412.
2. Crosbie EJ, Einstein MH, Franceschi S, Kitchener HC. Human papillomavirus and cervical cancer. *Lancet* 2013; 382: 889-899.
3. Woodman CB, Collins SI, Young LS. The natural history of cervical HPV infection: unresolved issues. *Nat Rev Cancer* 2007; 7: 11-22.
4. Rathinam VA, Fitzgerald KA. Innate immune sensing of DNA viruses. *Virology* 2011; 411: 153-162.
5. Scheffner M, Huibregtse JM, Vierstra RD, Howley PM. The HPV-16 E6 and E6-AP complex functions as a ubiquitin-protein ligase in the ubiquitination of p53. *Cell* 1993; 75: 495-505.
6. Boyer SN, Wazer DE, Band V. E7 protein of human papilloma virus-16 induces degradation of retinoblastoma protein through the ubiquitin-proteasome pathway. *Cancer Res* 1996; 56: 4620-4624.
7. Frye RA. Characterization of five human cDNAs with homology to the yeast SIR2 gene: Sir2-like proteins (sirtuins) metabolize NAD and may have protein ADP-ribosyltransferase activity. *Biochem Biophys Res Commun*

1999; 260: 273-279.

8. Imai S, Armstrong CM, Kaeberlein M, Guarente L. Transcriptional silencing and longevity protein Sir2 is an NAD-dependent histone deacetylase. *Nature* 2000; 403: 795-800.

9. Brunet A, Sweeney LB, Sturgill JF, Chua KF, Greer PL, Lin Y *et al*. Stress-dependent regulation of FOXO transcription factors by the SIRT1 deacetylase. *Science* 2004; 303: 2011-2015.

10. Rodgers JT, Lerin C, Haas W, Gygi SP, Spiegelman BM, Puigserver P. Nutrient control of glucose homeostasis through a complex of PGC-1alpha and SIRT1. *Nature* 2005; 434: 113-118.

11. Gillum MP, Kotas ME, Erion DM, Kursawe R, Chatterjee P, Nead KT *et al*. SirT1 regulates adipose tissue inflammation. *Diabetes* 2011; 60: 3235-3245.

12. Wang C, Chen L, Hou X, Li Z, Kabra N, Ma Y *et al*. Interactions between E2F1 and SirT1 regulate apoptotic response to DNA damage. *Nat Cell Biol* 2006; 8: 1025-1031.

13. Yeung F, Hoberg JE, Ramsey CS, Keller MD, Jones DR, Frye RA *et al*. Modulation of NF-kappaB-dependent transcription and cell survival by the SIRT1 deacetylase. *EMBO J* 2004; 23: 2369-2380.

14. Velez-Perez A, Wang XI, Li M, Zhang S. SIRT1 overexpression in cervical squamous intraepithelial lesions and invasive squamous cell carcinoma. *Hum Pathol* 2017; 59:

102-107.

15. Wang J, YujingWang, Liu C, Yu H. The effects of siRNA SIRT1 on the proliferation of human cervical cancer cells. *Int J of Sciences* 2016; 5: 133-136.

16. Singh S, Kumar PU, Thakur S, Kiran S, Sen B, Sharma S *et al*. Expression/localization patterns of sirtuins (SIRT1, SIRT2, and SIRT7) during progression of cervical cancer and effects of sirtuin inhibitors on growth of cervical cancer cells. *Tumour Biol* 2015; 36: 6159-6171.

17. In HY, Cao L, Mostoslavsky R, Lombard DB, Liu J, Bruns NE *et al*. A role for the NAD-dependent deacetylase Sirt1 in the regulation of autophagy. *Proc Natl Acad Sci U S A* 2007; 105: 3374-3379.

18. Bergsbaken T, Fink SL, Cookson BT. Pyroptosis: host cell death and inflammation. *Nat Rev Microbiol* 2009; 7: 99-109.

19. Fink SL, Bergsbaken T, Cookson BT. Anthrax lethal toxin and Salmonella elicit the common cell death pathway of caspase-1-dependent pyroptosis via distinct mechanisms. *Proc Natl Acad Sci U S A* 2008; 105: 4312-4317.

20. Yu J, Nagasu H, Murakami T, Hoang H, Broderick L, Hoffman HM *et al*. Inflammasome activation leads to Caspase-1-dependent mitochondrial damage and block of mitophagy. *Proc Natl Acad Sci U S A* 2014; 111: 15514-15519.

21. Fink SL, Cookson BT. Caspase-1-dependent pore formation during pyroptosis leads to osmotic lysis of infected host macrophages. *Cell Microbiol* 2006; 8: 1812-1825.

22. Zimmerman EM, Vaituzis Z, Hetrick FM. Mitochondrial damage and inhibition of respiration in animal cell cultures treated with Triton WR-1339. *J Cell Physiol* 1969; 74: 67-76.

23. Balaban RS, Nemoto S, Finkel T. Mitochondria, oxidants, and aging. *Cell* 2005; 120: 483-495.

24. Bergsbaken T, Fink SL, den Hartigh AB, Loomis WP, Cookson BT. Coordinated host responses during pyroptosis: caspase-1-dependent lysosome exocytosis and inflammatory cytokine maturation. *J Immunol* 2011; 187: 2748-2754.

25. Miao EA, Rajan JV, Aderem A. Caspase-1-induced pyroptotic cell death. *Immunol Rev* 2011; 243: 206-214.

26. Allison SJ, Jiang M, Milner J. Oncogenic viral protein HPV E7 up-regulates the SIRT1 longevity protein in human cervical cancer cells. *Aging* 2009; 1: 316-327.

27. Zhang D, Li S, Cruz P, Kone BC. Sirtuin 1 functionally and physically interacts with disruptor of telomeric silencing-1 to regulate alpha-ENaC transcription in collecting duct. *J Biol Chem* 2009; 284: 20917-20926.

28. Pfister JA, Ma C, Morrison BE, Dmello SR. Opposing effects of sirtuins on neuronal survival: SIRT1-mediated neuroprotection is independent of its deacetylase activity. *PLoS One* 2008; 3: e4090.

29. Campagna M, Herranz D, Garcia MA, Marcos-Villar L, Gonzalez-Santamaria J, Gallego P *et al*. SIRT1 stabilizes

PML promoting its sumoylation. *Cell Death Differ* 2011; 18: 72-79.

30. Hornung V, Ablasser A, Charrel-Dennis M, Bauernfeind F, Horvath G, Caffrey DR *et al*. AIM2 recognizes cytosolic dsDNA and forms a caspase-1-activating inflammasome with ASC. *Nature* 2009; *458*: 514-518.
31. Rathinam VA, Vanaja SK, Fitzgerald KA. Regulation of inflammasome signaling. *Nat Immunol* 2012; 13: 333-342.
32. Man SM, Karki R, Kanneganti TD. AIM2 inflammasome in infection, cancer, and autoimmunity: Role in DNA sensing, inflammation, and innate immunity. *Eur J Immunol* 2016; 46: 269-280.
33. Wilson JE, Petrucelli AS, Chen L, Koblansky AA, Truax AD, Oyama Y *et al*. Inflammasome-independent role of AIM2 in suppressing colon tumorigenesis via DNA-PK and Akt. *Nat Med* 2015; 21: 906-913.
34. Ma X, Guo P, Qiu Y, Mu K, Zhu L, Zhao W *et al*. Loss of AIM2 expression promotes hepatocarcinoma progression through activation of mTOR-S6K1 pathway. *Oncotarget* 2016; 7: 36185-36197.
35. Chen IF, Ou-Yang F, Hung JY, Liu JC, Wang H, Wang SC *et al*. AIM2 suppresses human breast cancer cell proliferation in vitro and mammary tumor growth in a mouse model. *Mol Cancer Ther* 2006; 5: 1-7.
36. Reinholz M, Kawakami Y, Salzer S, Kreuter A, Dombrowski Y, Koglin S *et al*. HPV16 activates the AIM2 inflammasome in keratinocytes. *Arch Dermatol Res* 2013; 305: 723-732.

37. Raposo G, Stoorvogel W. Extracellular vesicles: exosomes, microvesicles, and friends. *J Cell Biol* 2013; 200: 373-383.

38. Tetta C, Ghigo E, Silengo L, Deregibus MC, Camussi G. Extracellular vesicles as an emerging mechanism of cell-to-cell communication. *Endocrine* 2013; 44:11-19.

39. Akers JC, Gonda D, Kim R, Carter BS, Chen CC. Biogenesis of extracellular vesicles (EV): exosomes, microvesicles, retrovirus-like vesicles, and apoptotic bodies. *J Neurooncol* 2013; 113: 1-11.

40. de Rivero Vaccari JP, Brand F, Adamczak S, Lee SW, Perez-Barcena J, Wang MY *et al*. Exosome-mediated inflammasome signaling after central nervous system injury. *J Neurochem* 2016; 136 Suppl 1:39-48.

41. Waggoner SE. Cervical cancer. *Lancet* 2003; 361: 2217-2225.

42. Koh WJ, Greer BE, Abu-Rustum NR, Apte SM, Campos SM, Chan J *et al*. Cervical cancer. *J Natl Compr Canc Netw* 2013; 11: 320-343.

43. Gadducci A, Tana R, Cosio S, Cionini L. Treatment options in recurrent cervical cancer. *Oncol Lett* 2010; 1: 3-11.

44. Davidson S. Treatment for advanced cervical cancer: impact on quality of life. *Crit Rev Oncol Hematol* 2011; 79: 24-30.

45. Kamura T, Ushijima K. Chemotherapy for advanced or recurrent cervical cancer. *Taiwan J Obstet Gynecol* 2013; 52: 161-164.

# 국문 초록

포유류 세포들은 바이러스에 대항하는 선천 면역계를 지니고 있다. 인유두종 바이러스에 감염된 자궁경부암세포는 자신의 생존과 성장을 위해서 숙주의 이러한 항바이러스 선천 면역 방어체계를 극복해야만 한다. 하지만, 아직까지 자궁경부암세포가 항바이러스 면역체계를 회피하는 기전은 완전히 밝혀지지 않았다. 본 연구진은 Sirtuin 1 (SIRT1)이 인유두종 바이러스에 감염된 자구경부암세포에서 특이적으로 과발현 되어 있는 것을 주목하였고, SIRT1이 항바이러스 선천 면역체계에 대응할 것으로 가설을 세웠다. 자궁경부암세포에서 과발현 되어 있는 SIRT1을 억제 했을 때, 강력한 암세포 사멸이 일어났으며 이러한 효과는 SIRT1이 회복 됐을 때 상쇄 되었다. SIRT1이 억제되어 사멸하는 자궁경부암세포는 Absent in melanoma (AIM2)와 염증조절 복합체의 하위 유전자들이 크게 발현되는 pyroptosis라는 세포사멸기전의 대표적인 특징들을 보였다. 기전적으로는, SIRT1이 NF-κB의 구성 인자 중 하나인 RELB의 mRNA의 불안정화를 유도함으로써, NF-κB에 의해 전사 되는 AIM2를 억제한다. 놀랍게도, pyroptosis 세포 사멸 신호는 pyroptosis로 사멸되는 암세포 자신 뿐만 아니라 AIM2-염증조절 복합체와 관련된 단백질들을 세포외 전달 물질을 통해 세포외로 분비해서 주변 자궁경부암세포 에게도 전달 되었다. 더욱이, 자궁경부암세포를 이종 이식한 마우스 모델에서도 SIRT1-표적 siRNA를 처치하거나, 자궁경부암세포에서 SIRT1을 억제한 뒤 획득한 세포외 전달물질을 처치한 군 모두에서 자궁경부암세포의 성장을 억제하는

것을 확인하였다. 임상적으로는, 자궁경부암 환자의 조직을 이용한 면역조직화학 염색 분석을 통해 SIRT1의 발현이 많을수록 환자들의 부정적인 예후와 상관관계가 있는 것을 확인하였다. 결과적으로, SIRT1은 인유두종 바이러스에 감염된 자궁경부암세포가 AIM2-염증조절 복합체에 의한 항바이러스 면역 체계를 무력화 시켜서 암세포의 성장을 돕는다. SIRT1이 없이는, 자궁경부암세포는 AIM2-염증조절 복합체에 의한 항바이러스 면역 체계의 억제 실패로 인하여 더 이상 생존할 수 없으므로, SIRT1은 자궁경부암의 치료에 있어서 획기적인 치료 표적이 될 수 있을 것으로 기대한다.

---

**주요어: 자궁경부암, 인유두종 바이러스, 염증조절 복합체, Sirtuin 1, Absent In Melanoma 2, , Pyroptosis**

**학 번 : 2012-23667**